UNIVERSITY OF CALIFORNIA SAN DIEGO

The Role of CA3 Sharp-wave Ripples in Spatial Working Memory on a Dentate-Dependent 8-Arm Radial Maze Task

A Thesis submitted in partial satisfaction of the requirements

for the degree Master of Science

in

Biology

by

Brandon Taylor

Committee in charge:

Professor Jill Leutgeb, Chair
Professor Stefan Leutgeb, Co-Chair
Professor Jon Christopher Armour

2022

The thesis of Brandon Taylor is approved, and it is acceptable in quality and form for publication on microfilm and electronically.

University of California San Diego 2022

DEDICATION

To my parents, thank you for all of the support and guidance throughout the years. I truly could not have done it without your continued presence. I hope I have made you proud!

To my friends and family, I am deeply grateful for all of the kind words and nice deeds you passed on to me throughout this long year in the BS/MS program. You all kept me going when times were tough, and I will be forever thankful.

TABLE OF CONTENTS

LIST OF ABBREVIATIONS

SWR	Sharp-wave ripple
SW	Sharp-wave
LTP	Long-term potentiation
WM	Working memory
MTL	Medial temporal lobe
MEC	Medial entorhinal cortex
LFP	Local field potential
SD	Standard deviation
DG	Dentate gyrus
SR	Stratum radiatum
vHC	Ventral hippocampal commissure
NS	No-stimulation trial blocks
S	Stimulation trial blocks
Cheetah	Digital Neuralynx recording software
I/O curve	Input-output curve
PBS	Phosphate buffered saline
PFA	Paraformaldehyde
D&S	SWR detection & vHC stimulation
H-Bc	Holm-Bonferroni correction
N.S.	Not statistically significant

LIST OF FIGURES & TABLES

ACKNOWLEDGEMENTS

I would like to acknowledge Professor Jill Leutgeb for her assistance throughout all aspects of this project. Her guidance, mentorship, and thesis revisions were extremely valuable throughout this process.

I would also like to acknowledge Yuhan Zhang for her computational support throughout this project. Her programs made it possible to detect and disrupt SWR events during the behavioral task. In addition to that, it was through her efforts that we were able to calculate the related SWR efficiency for all conducted experiments.

I would also like to acknowledge Professor Stefan Leutgeb for his technical assistance throughout this project. Most notably, he always conducted the lengthy surgical operations that were necessary to collect any of the data presented in this thesis.

This thesis is currently being prepared for submission of publication of the material by Zhang, Yuhan; Taylor, Brandon; Leutgeb, Stefan; Leutgeb, Jill. The author of this thesis will be a co-author of the publication.

ABSTRACT OF THE THESIS

The Role of CA3 Sharp-wave Ripples in Spatial Working Memory on a Dentate-Dependent 8-Arm Radial Maze Task

by

Brandon Taylor

Master of Science in Biology

University of California San Diego, 2022

Professor Jill Leutgeb, Chair
Professor Stefan Leutgeb, Co-Chair

The hippocampus plays a fundamental role in the immediate processing of afferent information from many brain regions and has been linked to emotional regulation, learning and memory formation, and spatial processing. Decoded neuronal activity during sharp-wave ripple (SWR) events has shown how hippocampal place cells are activated during SWRs, and these place cells code for future goal locations. Additionally, these future goal locations on complex spatial WM tasks are no longer represented during SWR events when the dentate gyrus (DG) is

lesioned, leading us to hypothesize that SWR events generated in the CA3 region of the hippocampus are necessary for guiding ongoing spatial working memory (WM) behavior. We analyzed the real-time local field potential (LFP) for SWRs while animals performed a complex spatial WM task, and we electrically stimulated the ventral hippocampal commissural fibers to induce transient silencing of pyramidal neurons in CA1 and CA3 to prevent place cell reactivation during SWR events. Disruption of CA3 SWRs did not cause any significant spatial WM performance deficits compared to controls, suggesting that CA3 SWRs are not causally linked to spatial WM processes. Therefore, contrary to this popular belief in the field, our results indicate SWR events are not the primary mechanism for guiding hippocampal-dependent spatial WM behavior.

INTRODUCTION

Memory Formation and Storage in the Brain

Memory is defined as a process by which what is learned persists over time. Memories can be classified as short-term or long-term, depending on the stability of that memory over time. The search for where memories are formed or stored has been a primary goal in neuroscience research ever since the early 20th century. One psychologist by the name of Karl Lashey explored this question in 1950 by inducing cerebral cortex lesions on rats that have previously learned to navigate a spatial maze. He was searching for evidence of the "engram" (also commonly referred to as the memory trace), which is a hypothetical physical storage site for memories in the brain. It turned out that the location of the lesion had no correlation with the rats' abilities to complete the maze, but the extent of the lesion correlated with the rats' impaired ability to remember the maze. Lashley concluded that there was no evidence of an engram, but that memory was distributed widely throughout the cortex (Lashley, 1950). Further evidence for this idea began to emerge in the late 1930's from the work of an American-Canadian neurosurgeon named William Penfield who was removing diseased tissue from the medial temporal lobe (MTL) of patients with recurrent epileptic seizures (Penfield & Boldrey, 1937). Penfield found that, upon electrical stimulation to the MTL, patients experienced vivid recapitulations of prior memories they had experienced. Additionally, removal of the brain tissue did not wipe out the trace of the memory for a particular experience. These findings suggested that cortical structures within the MTL may be responsible for controlling some aspects of memory, although it appears these memories do not seem to be stored specifically in the MTL.

The Role of the Hippocampus in Memory Formation and Storage

The hippocampus is a brain region that lies deep within the MTL. Evidence that the hippocampus plays a role in memory formation comes from the infamous case-studies of patients E.P. and Henry Gustav Molaison (H.M.). E.P. contracted viral encephalitis that bilaterally destroyed his medial temporal lobes, causing complete anterograde amnesia with temporally-graded retrograde amnesia (Insausti et al., 2013). Despite sustaining severe memory impairments, other aspects of E.P.'s cognitive function such as working memory, spatial navigation, and frontal lobe function remained intact. (Insausti et al., 2013). Patient H.M. sustained a head injury after a bicycle accident as a young child, ultimately developing incapacitating seizures by his teenage years. American neurosurgeon William Scoville performed a bilateral hippocampal resection, a radical procedure which involved the removal of both hippocampal hemispheres from H.M.'s brain in an attempt to control the seizures (Penfield & Milner, 1958). The seizures contracted, but H.M. was left with permanent anterograde amnesia, rendering him unable to form any new declarative memories. However, he retained distant long-term memories that were commonly associated with childhood. For example, he remembered his old house address perfectly, but once his family moved to a new location after his surgery, he failed to commit the new location to memory and could not navigate back to the new house on his own (Penfield & Milner, 1958). Although H.M. was unable to form new declarative memories, his ability to learn new visuomotor skills remained intact (Squire, 2009). These two case-studies demonstrated several things about memory and the brain. First, it became clear that two main types of memories exist: explicit and implicit, and each type is carried out by a different brain region. Additionally, this observation demonstrated that the hippocampus and surrounding cortical regions play a crucial and necessary role in the formation of new declarative

memories (Penfield & Milner, 1958). Later studies investigating the role of the hippocampus would demonstrate that hippocampal-lesioned rodents take significantly longer to complete the Morris Water Maze task, concluding that the hippocampus also controls aspects of spatial memory (Morris et al., 1982).

Anatomy and Functions of the Hippocampal Subregions

The hippocampus is a unique cortical region that lies deep within the MTL of both hemispheres of the brain. It can be subdivided into four main subregions: CA1, CA2, CA3, and the DG (Schultz & Engelhardt, 2014). The neurons in these regions are densely populated, forming a pyramidal cell layer that extends from the CA1 to CA3 region (Figure 1). The CA regions differ from one another in several ways. The CA2 region exhibits lower levels of calcium, potentially explaining the lack of synaptic plasticity observed at the stratum-radiatum (SR)-CA2 synapse (Dudek et al., 2016). Additionally, the CA1 and CA3 regions exhibit widely different genomic profiles, with more than 1000 uniquely expressed genes in each region (Newrzella et al., 2007). Another difference between the CA regions involves the connectivity between hippocampal and cortical regions. Axonal projections from layer II of the entorhinal cortex primarily synapse in the molecular layer of the DG, forming the perforant path (Amaral et. al., 2007). All projections from the DG have one downstream target, synapsing near the cell bodies of the CA3 neurons through the mossy fiber path (Green, 1964). CA3 pyramidal neurons loop back to project onto themselves, forming a recurrent network (Green, 1964). Additionally, CA3 neurons project via the Schaffer collateral pathway to the dendrites of the CA1 neurons (Green, 1964). Finally, CA1 neurons project axons out of the hippocampus to several brain regions, including the subiculum, amygdala, perirhinal, prefrontal, and entorhinal cortices (Groen & Wyss, 1990). Anatomical differences between the three CA regions leads to functional

differences. CA1 has been hypothesized to play a role in input integration while the CA3 region is involved with pattern completion processes (Yamada & Jinno, 2021). Inactivation of neurons in the CA2 region has revealed a necessary role for the CA2 region in social memory (Hitti & Siegelbaum, 2014). All together, the CA regions of the hippocampus work to form a trisynaptic loop of information that is thought to contribute to many memory processes.

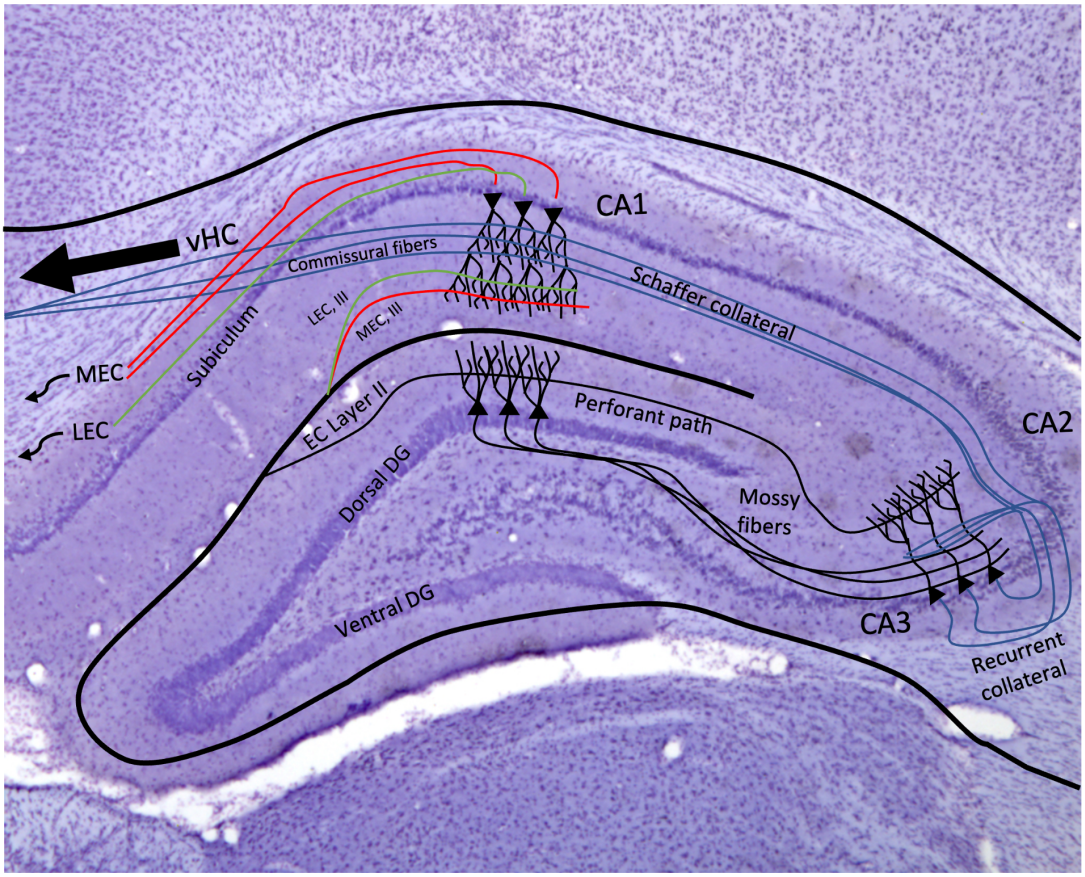

Figure 1. Anatomy and Connectivity of the Hippocampal Subregions. Layer II entorhinal inputs from the medial entorhinal cortex (MEC) and lateral entorhinal cortex (LEC) converge to form the perforant path, which synapses on dendrites of the DG and CA3 regions. The DG projects to the CA3 region through the mossy fiber pathway. CA3 neurons synapse onto dendrites of the CA1 region, forming the Schaffer collateral pathway. CA3 neurons also form a recurrent collateral circuit where they loop back and project onto themselves as well as the other CA3 region in the opposite hippocampal hemisphere. Layer III entorhinal inputs from MEC and LEC project onto separate regions of CA1 dendrites. CA1 and subiculum neurons project back in register to the deep regions (layer V, VI) of the entorhinal cortices and surrounding MTL structures. In addition to the Schaffer collateral and recurrent collateral pathways, CA3 axons also project to the opposing hippocampal hemisphere through the commissural fibers leading to the ventral hippocampal commissure (vHC).

Role of the Dentate Gyrus in Spatial Working Memory

A ground-breaking discovery was made recently when researchers discovered the presence of cells that fire in a unique grid pattern in the medial entorhinal cortex (MEC). These "grid cells" fire in a periodic pattern that forms a repeating grid of equilateral triangles, allowing an animal to navigate its environment through simple distance calculations based on the firing patterns of a single cell (Hafting et al., 2005). This finding, along with the existence of border cells (Solstad et al., 2008), head-direction cells (Killian et al., 2012), speed cells (Dannenberg et al., 2019) and time cells (MacDonald et al., 2011) provides strong evidence that the MEC serves as a navigational hub for the brain. In addition to the MEC exists the lateral entorhinal cortex (LEC); this region is thought to provide unimodal sensory input to the hippocampus (Knierim et al., 2013). The MEC and LEC form converging input streams that project into all hippocampal CA formations, including the DG subregion (Witter et al., 2017). Therefore, the hippocampus functions to receive and integrate direct sensory-related inputs from cortical regions. Since the DG only synapses onto the cell bodies of CA3 pyramidal neurons (Green, 1964), it is often considered to be the initial step in the unidirectional trisynaptic hippocampal circuit that is thought to strongly contribute to the formation of episodic memories (Amaral et al., 2007).

One important role that the DG has been shown to facilitate is pattern separation, which is the ability to form discrete neuronal representations based on the presentation of similar stimuli (Leutgeb et al., 2007). This is thought to occur when small changes in the environment are represented by unique rate patterns among the sparsely-firing granule cells (Leutgeb et al., 2007). This provides a potential mechanism that explains how memory encoding can lead to the formation of distinctly stored memories. In addition to pattern separation, the DG has also been known to support spatial WM processes (Xavier & Costa, 2009). Spatial WM refers to the ability

to temporarily hold spatial information in working memory; this cortical computation allows an individual to flexibly use information to navigate an environment or perform a certain behavior. Granule-cell-specific lesions induced by colchicine administration have led to impaired performance on the eight-arm radial maze, confirming that the intact DG is necessary for spatial WM processes (McLamb et al., 1988; McNaughton et al., 1989; Walsh et al., 1986, as cited in Xavier & Costa, 2009).

Hippocampal Oscillations

The DG and CA hippocampal subregions work harmoniously together to process and integrate incoming stimuli to support the formation of episodic memories. In order to do this, the hippocampal trisynaptic circuit must generate three main oscillatory events: theta oscillations, gamma oscillations, and sharp-wave ripples (SWRs) (Butler & Paulsen, 2015). Theta oscillations generally fall within a frequency range of 4-12 Hz, and they are known to occur during periods of movement, activity, and REM sleep (Nuñez & Buño, 2021). These oscillations occur ubiquitously throughout the neocortex and hippocampus alike. Gamma oscillations (25-140 Hz) are observed in short bursts during alert behaviors and are thought to synchronize neuronal assemblies in times where higher-order hippocampal computations may be taking place (Colgin & Moser, 2010). Finally, SWRs are the most synchronous pattern of neural activity in the mammalian hippocampus. SWRs are generated in the CA3 region, with modulation coming from the DG and CA2 regions (Sasaki et al., 2018; Oliva et al., 2016). CA3 SWRs then propagate to the CA1 region, where they are observed on the LFP (Buzsáki, 2015). These oscillations are often characterized as events that cross a threshold of 3-9 standard deviations above the 150-250 Hz bandpass-filtered mean LFP amplitude activity (Joo & Frank, 2018). These ripples occur

while the brain is in an offline state, such as during periods of non-REM sleep, immobility, and consummatory behaviors (Joo & Frank, 2018).

Place Cells and Place Fields

John O'Keefe (1976) discovered a special type of cell in the rat hippocampus that seemed to represent and code for spatial information. These "place cells" preferentially increased their firing rates when the animal was in a very specific location on a maze. These locations are known as "place fields," and they represent locations where corresponding place cells will reliably increase their firing rates upon entry into that location. In addition to spatial information, place cells can also code for other non-spatial information (Leutgeb et al., 2005). Non-spatial features such as box shape or color can be represented by different firing rates, even while the place cell's location-dependent activation remains the same. When considered all together, these findings provide clear evidence that the hippocampus plays a significant role in processing both spatial and non-spatial memory.

Functional Role of SWRs

The synchronous activation of a large number of hippocampal pyramidal neurons during SWR events has been long theorized to facilitate long-term potentiation (LTP), or the strengthening of synaptic connections leading to increased synaptic transmission over time. LTP can be induced by high-frequency stimulation of presynaptic axons causing coincident depolarization of postsynaptic neurons (Bliss & Collingridge, 1993). This theory was confirmed for the first time in-vivo in 2006 when researchers trained rats on an inhibitory avoidance task that facilitated the formation of associative memory (Whitlock et al., 2006). Rats that learned to associate the dark segment of the experimental box with a foot shock demonstrated enhanced synaptic plasticity in the CA1 region of the hippocampus as measured by a multi-electrode array

setup. Additionally, the researchers found that this synaptic plasticity was saturable. Rats that had previously demonstrated plasticity enhancements during the task showed significantly weaker responses to artificial electrode stimulation when compared to control rats that had not previously learned to associate the dark with the shock. These findings strongly supported the conclusion that memories are stored on a cellular level through the formation of enhanced synaptic communication between neurons in the brain. These in-vivo findings would also later be supported by in-vitro analysis by Josef et al. (2016), who showed that SWRs facilitate coincident depolarization between CA3 and CA1 place cells, ultimately resulting in enhanced synaptic plasticity in-vitro. These discoveries highlight how SWRs facilitate synaptic plasticity processes to strengthen memory traces.

SWRs also have been shown to facilitate the reactivation of place cell spiking activity in a time-compressed sequence (Nádasdy et al., 1999). This retrieval of neuronal representations has been hypothesized to contribute to memory consolidation processes through repeated hippocampal-cortical-hippocampal information loops that strengthen synaptic plasticity (Joo et al., 2018). Additionally, some studies have analyzed the content of SWR events. Upon analysis of place cell activity during awake behavior, Foster & Wilson (2006) discovered that place cell activity is replayed in a reverse manner immediately after rats ran on linear and U-track mazes. Additionally, these reverse replay events were found to be coincident with SWRs occurring during awake behavior (Foster & Wilson, 2006). Future experiments by Pfeiffer & Foster (2013) would later provide evidence that place cell sequences are reactivated during SWRs and that these sequences depict spatial trajectories towards known goal locations. Due to the content and modulation of these different replay mechanisms, reverse replay events have been hypothesized to contribute towards a consolidation mechanism while forward replay events are thought to

guide future navigational behavior and planning (Joo et al., 2018). The hippocampal SWR is therefore a popular candidate for supporting various cognitive functions.

Lesions and behavioral studies previously discussed (McLamb et al., 1988; McNaughton et al., 1989; Walsh et al., 1986, as cited in Xavier & Costa, 2009) described that the DG was necessary for spatial WM tasks, but the findings presented by Sasaki et al. (2018) were the first to shed light on a potential mechanism for how this happened. CA3 place cells containing place fields for future reward arms became preferentially activated during SWR events after reward consumption. These CA3 SWR events were mediated by and dependent upon DG-related input, and removal of the DG resulted in reduced SWR generation upon reward consumption. Finally, these CA3 SWRs contain place cell sequences that code for future reward locations (Sasaki et al., 2018). When taken together, these findings suggest that CA3 SWRs facilitate the retrieval of neuronal information that supports memory-guided behavior, and these dynamics rely upon the intact functional activity of the DG.

Disruption of SWRs Leads to Learning and Memory Impairments

All of the previous studies have demonstrated the content and potential functions of SWRs in awake, live-behaving animals. Yet none of them have developed a causal relationship between SWR function and memory consolidation. Girardeau et al. (2009) were the first to do this by selectively detecting and electrically disrupting SWRs during the consolidation period after behavioral testing on a version of the eight-arm radial maze where the same three arms were baited with reward each day. Test rats receiving one hour of SWR disruption following behavioral training on the radial maze showed impaired learning and worse memory performance on the maze task when measured each day when compared to unimplanted animals and delayed-stimulation control animals. The team concluded that SWRs were necessary for

memory consolidation, presumably due to the temporally-compressed neuronal activation that occurs during ripple events that is known to facilitate synaptic plasticity.

Another study conducted by Jadhav et al. (2012) considered the effects that awake SWR activity has on spatial memory and learning. Using an online-feedback loop system, the team was able to detect awake SWRs while a rat traversed a W-track spatial alternation maze. SWR-disrupted animals performed significantly worse than delayed-stimulation control and unstimulated animals on the outbound component of the hippocampal-dependent W-track maze when tested over a time period of eight days. This finding suggested a functional role for awake SWRs in spatial memory and learning. When considered together, these two studies demonstrate a clear role for SWRs in learning and memory processes during sleep and wakefulness.

Goal of the Project

SWRs have intrigued neuroscience researchers ever since their discovery in 1969. Since this time, studies have demonstrated their existence in rodents, primates, and humans. They primarily occur when the brain is in an offline state (Joo et al., 2018), and they are thought to play a role in many memory processes. The functional role of SWRs in learning and consolidation has been repeatedly demonstrated as interruption of ripple events results in slower learning and impaired memory retention. Research in epileptic human patients has shown that these ripple events proceeded and facilitated cognitive processes that allowed for the spontaneous retrieval of previously encoded memories (Norman et al., 2019).

Sasaki et al. (2018) showed that the DG is necessary for spatial WM tasks due to its ability to mediate and coordinate ripple-related events in the CA3 region of the hippocampus. My research project will expand upon this previous work by seeking to uncover the causal relationship that exists between the CA3 SWR and ongoing behavior in a dentate-dependent

spatial WM task. I will test the hypothesis that CA3-generated SWRs are required and necessary for correct decision-making during spatial WM tasks when inputs from the dentate gyrus to CA3 are necessary. In order to test this hypothesis, the experimental animals will be trained in the eight-arm radial maze, which assesses their spatial WM abilities and is dentate-dependent. The animals will then undergo drive-implantation surgery to position tetrodes above the hippocampus on one hemisphere of the brain. Over the next 1.5-2 weeks, these tetrodes will be manually turned down into cell populations in specific regions in the hippocampus, such as CA1, CA2, CA3, and the DG. These tetrodes will allow us to simultaneously record from several hippocampal regions while the animal is performing the maze task. Current-induced stimulation of the ventral hippocampal commissural (vHC) fibers leads to SWR disruption as well as temporary inhibition of CA1 cells in the hippocampus (Jadhav et al., 2012). I will use this stimulation to temporally inhibit hippocampal cells and subsequently block SWR generation during ongoing behavior. In addition, I will also conduct 200 ms delayed-stimulation control experiments that will allow the SWRs to propagate through the hippocampus before disruption occurs; this will also address if the stimulation itself accounts for any behavioral changes seen. I will employ a closed-loop experimental technique that will involve the real-time detection and immediate disruption of SWRs. I will screen for any changes or deficits in behavior that the animal displays while performing the task with and without SWRs. After behavioral training has been completed, the animal will be perfused in order to retrieve the brain for histology and microscopy. This will allow us to confirm with certainty that the tetrodes were placed in the regions that we were aiming for. Once this is confirmed, the data can be compared across animals for each experiment performed: no-stimulation, stimulation to disrupt SWRs, and delayed stimulation. This current study will seek to determine if CA3 SWRs play a causal role in

rodent spatial WM processes that have been shown to require input from the DG subregion of the hippocampus.

CHAPTER I–METHODS

Approvals

All implemented experimental and surgical procedures were pre authorized through the Institutional Animal Care and Use Committee at the University of California, San Diego. All methods were conducted at the University of California, San Diego in accordance with the National Institutes of Health guidelines.

Subjects

A total of nine male Long Evans rats (3-6 months old) were included in the analysis used in this study. All rats were ordered from Charles River Laboratory. The animals were each caged individually in an on-site vivarium on a 12/12hr reverse-light schedule. The animals were given approximately one week to become acquainted with their new environment while they slowly transitioned to a restricted food diet to maintain at or approximately 85% of their initial body weight. Access to drinking water was not limited.

Spatial WM behavioral task

All behavioral training took place on an eight-arm radial maze that consisted of a central circular platform (27 cm in diameter) with eight arms (79 cm x 12 cm) that was semi automated and controlled through the use of a remote switch (Sasaki et al., 2018). All animals were first habituated on the maze for daily 10-minute sessions with all arms freely available until they were comfortable traversing the maze and consuming the chocolate milk reward (0.2 mL). Chocolate milk rewards were located in the center of a raised circular ring at the end of each arm; the raised rings were intended to prevent the animal from visually identifying the presence of the reward until it had fully committed to running down the arm. The drop of milk was manually replaced by the researcher before the beginning of each trial. Milk drops were placed on the tips of reward

sensor wires that changed resistances when the animal licked up the reward, allowing for a visual computer confirmation that the animal was consuming a reward after traveling down an arm. Animals were selected for surgery if they mastered the habituation task without jumping off of the maze. These animals were taken off of food restriction for five days prior to surgery, during which point they are not trained or habituated.

After post-surgical recovery, animals were trained on the next phase of the behavioral task. Each trial begins with the animal on the center stem platform with all eight arms lowered and inaccessible. Each trial consists of a "forced phase" and a "choice phase," each of which contain four pseudorandomly ordered arm combinations that is decided prior to the start of each experiment, excluding instances where arms are presented in a spatial order (i.e., 1, 2, 3, 4). Additionally, each experiment is further divided up into "trial blocks" of typically 3 or 4 trials, depending on the total number of expected trials that will be run by the animal during each experimental day based on previous performance during post-surgical behavioral training. These trial blocks fall into two categories: "no-stim (NS)" control blocks or "stimulation" (S) manipulation blocks. During stimulation trials, bipolar current stimulation of the commissural fibers connecting the two hippocampal hemispheres will be triggered upon detection of a SWR in the designated CA region. This manipulation transiently silences SWR-associated pyramidal neuron firing in the CA regions, and it will be used to screen for spatial WM impairments while the animal traverses the 8-arm radial maze task. Each experiment alternates between NS and S trial blocks, always beginning and ending with a NS trial block. The forced phase of the behavior begins when the researcher, who sits on the opposite side of the room divided by a large curtain, manually flips a pressure-controlled switch to raise one of the arms to form a connected segment that the animal can then travel down to retrieve the reward at the end of the arm (Figure 2). After

the animal has eaten the reward, the next arm is raised and the animal travels down towards the next reward as the prior arm is lowered to preclude re-entry during the forced phase. Once the animal travels down the fourth arm and is finishing the reward, all remaining arms are simultaneously raised to begin the choice phase. The animal is expected to travel down the remaining four baited arms, with each re-entry into a previously explored arm counting as an error. The researcher watches the animal's behavior in real-time through a video camera fixed to the ceiling above the maze. Behavior can also be monitored through a light-tracking camera that is sensitive to the light-emitting diodes that are embedded into the hyperdrive fixed to the head of the animal. This camera tracks the X-Y coordinates of the animal and superimposes them over a computer-generated plot of the eight-arm radial maze to show the researcher the exact position of the animal's head and direction over time. Due to the hedging or peeking behavior that some animals exhibit while searching for the remaining baited arms, an error was only counted if the animal's head crossed the half-way point on each arm; this point is easily measurable and quantifiable as this is the pivot point for the arm to raise or lower. The trial ends once the animal retrieves all eight rewards and returns back to the center platform, or if total time exceeds ten minutes. Trials that exceed ten minutes are subsequently removed from analysis. After conclusion of a trial, an intertrial interval of two minutes was used to allow the researcher to bait each of the eight arms before the beginning of the next trial. Three to four trials make up each of the trial blocks, which are ordered NS1, S1, NS2, S2, NS3.

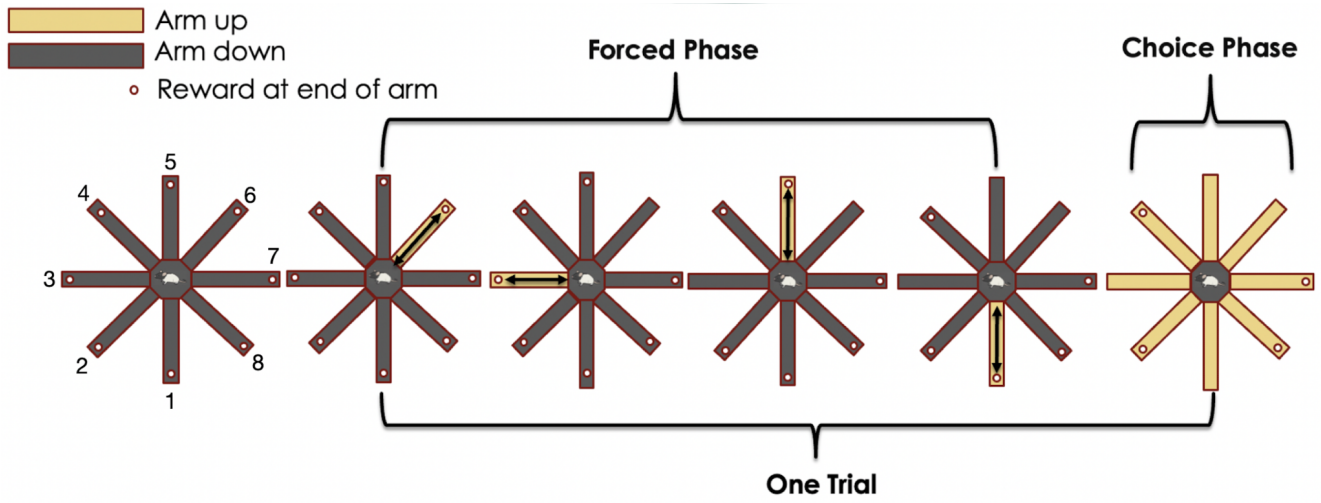

Figure 2. Spatial WM Task on the Eight-Arm Radial Maze. Each trial begins with the animal on the center platform with all arms lowered. The forced phase shows an example sequence (6, 3, 5, 1), followed by a choice phase where the animal is expected to visit arms 2, 4, 7, and 8 in any order (without visiting any of the previous arms) in order to receive a perfect score for that trial.

Surgical Hyperdrive Implantation

Animals that demonstrated proficiency during the habituation stages of training were selected for a single stereotaxic surgery that resulted in a chronic implantation of a multi-electrode hyperdrive positioned over one hippocampal hemisphere. The hyperdrive served as the housing unit for 14 independently movable tetrodes arranged in a tight bundle that feeds downwards through the post of the drive. Animals were fed ad libitum for five days prior to surgery. Animals were weighed on the day of surgery in order to calculate proper dosages for the anesthetic isoflurane gas (typically 2.0-2.5% with O_2) and analgesic buprenorphine (0.05 mg/kg). Eight to ten stainless steel screws were drilled partly through the skull in a circular pattern in order to fix the drive to the skull when dental cement was later applied. A pair of bipolar stimulating wires (one pair per hemisphere) were located 1.1 mm posterior and 1.3 mm lateral to bregma to position them over the vHC; they were subsequently lowered 3.6 mm deep into this region. The tetrode bundle was positioned over the right hippocampal hemisphere using

coordinates that were 4 mm posterior and 3 mm lateral to bregma. Tetrodes each consisted of 4 twisted wires (4-6 μm in diameter) that were plated in platinum prior to surgery to adjust the resistances to the desired range. Dental cement was applied to fix the drive to the skull and to cover the exposed wire cannulas belonging to the stimulation and ground wires that would be inserted into the drive. Animals were given at least five days of recovery after the surgery before behavioral training would resume.

Tetrode Turning

Tetrode turning begins right after surgery as the animal is waking up. The tetrode wires are each connected to an independently movable screw with a directional head that allows a specialized screwdriver to fit into place only when facing the same direction as the screw. All tetrodes are lowered three full clockwise "turns" following the surgery; each 360° turn represents a distance traveled of 320 μm. Directional coordinates (i.e., north, south, east, west) and depths are tracked for each of the tetrodes. For the first week of turning after surgery, tetrodes are first turned up in the counterclockwise direction ½ turn to free them from any debris or gliosis before they are advanced deeper into the brain. One day after surgery, all tetrodes would be advanced again by several hundred micrometers, usually equalling 1.5 turns. One of the reference tetrodes (R2) would be lowered down deeper than the others until characteristic hippocampal LFP oscillations such as sharp-waves (SW) and theta oscillations began to appear. R2 was never moved again so that it served as a reference for how much brain shifting and tetrode sliding occurred throughout the turning phase. Another reference tetrode (R1) will be left in the cortex at a depth of approximately 1600 μm to provide a differential reference to subtract away cortical signals from the desired hippocampal signals seen on the other tetrodes. All other tetrodes were slowly advanced to the hippocampal CA1 layer. Auditory markers, visual LFP patterns, and

tetrode depths were carefully tracked as tetrodes neared the CA1 pyramidal cell layer (Figure 3). Positive (downward-deflection) SWs with ripples are seen as tetrodes hover above the CA1 cell layer (Figure 3A), (Buzsáki, 2015). As tetrodes are turned into the cell layer, the SWRs become flat (Figure 3B) before eventually reversing polarity into negative (upward-deflection) sharp-waves with ripples at tetrodes pass through the bottom side of the CA1 cell layer (Figure 3C). After all tetrodes have reached the CA1 layer, a majority of the tetrodes will be designated as CA3 tetrodes and will be turned through CA1 down towards the CA3 layer over a time period of approximately 10 days. CA1 tetrodes are initially turned up and will be lowered in parallel as CA3 tetrodes approach their respective cell layer to allow for simultaneous CA1/CA3 LFP recordings. Tetrode depths and spike multiunit activity are carefully tracked while the tetrodes are turned through the SR and DG molecular layer towards the CA3 cell layer. Tetrodes are advanced in small increments as they near the CA3 cell layer (Figure 3D) where larger pyramidal neurons can be observed along with large-amplitude SWR oscillations. Tetrodes are allowed to slowly settle into the layer to increase recording stability to allow for several recording days to be conducted. Final tetrode locations will be confirmed during post-mortem histological analysis.

Figure 3. CA1 and CA3 SWRs Recorded on the Hippocampal LFP. A, Downward (+) SW deflections with ripple are recorded on a tetrode that is positioned right above the CA1 cellular layer. **B,** SWR oscillations become more flat as the tetrode is lowered into the CA1 layer. **C,** Upward (-) deflection SWs with ripple are observed as the tetrode moves below the CA1 layer. D, Reversed-polarity (-) SWRs are simultaneously recorded on several tetrodes nearing the CA3 cell layer.

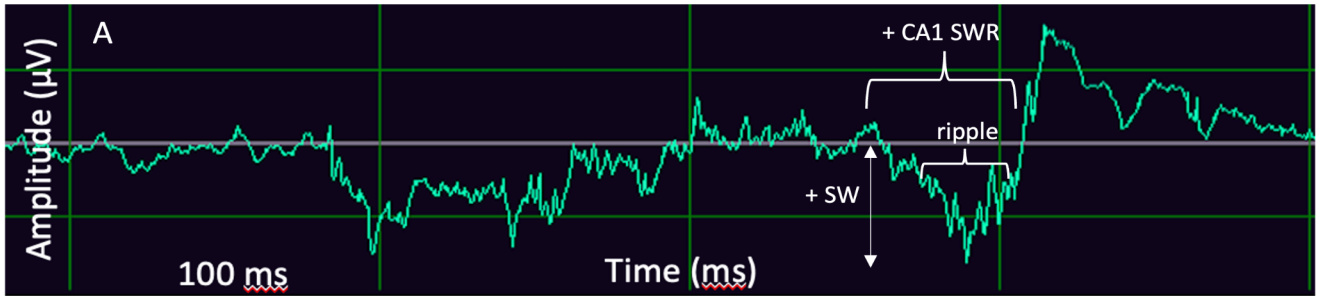
A
+ CA1 SWR
ripple
+ SW
Amplitude (µV)
100 ms
Time (ms)

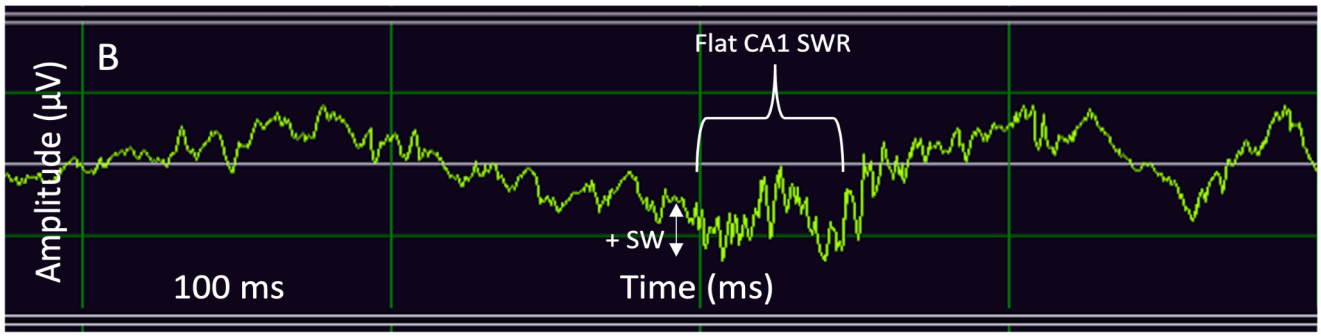
B
Flat CA1 SWR
+ SW
Amplitude (µV)
100 ms
Time (ms)

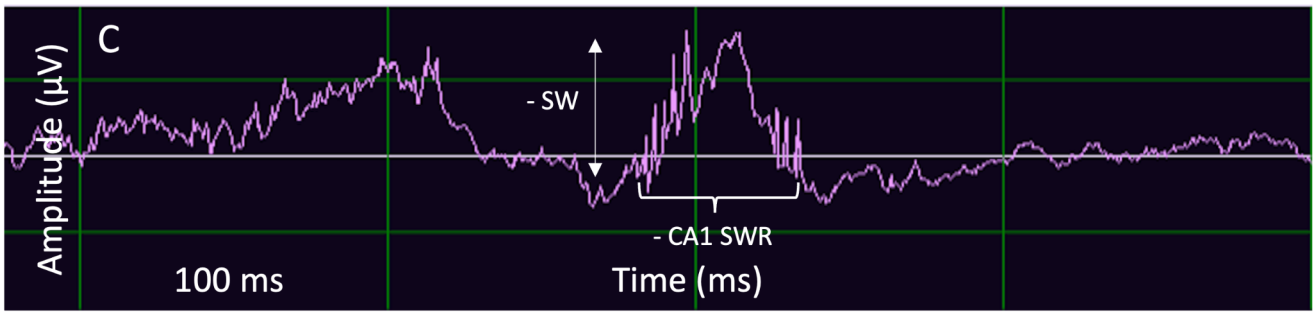
C
- SW
- CA1 SWR
Amplitude (µV)
100 ms
Time (ms)

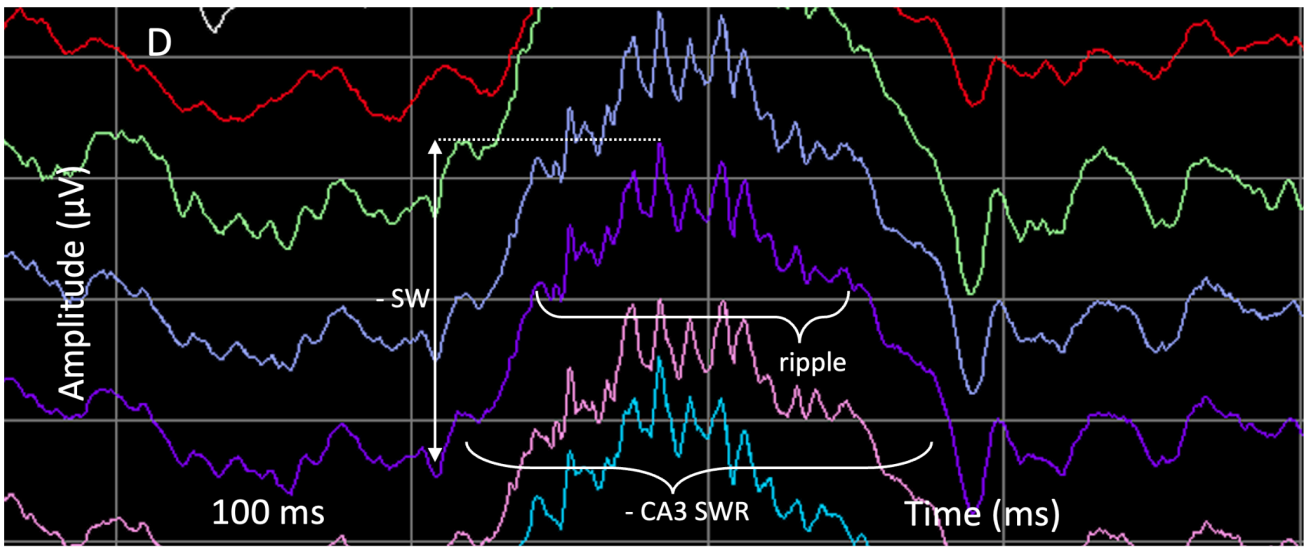
D
- SW
ripple
- CA3 SWR
Amplitude (µV)
100 ms
Time (ms)

Recording Apparatus

The animal's hyperdrive is connected through a bundle of wires to the physical Neuralynx recording apparatus. The digital Neuralynx software (Cheetah) allows for real-time visualization of the LFP and spike multiunit activity. Xilinx software is used in tandem with Cheetah to monitor and detect SWR activity on up to four tetrode channels (assigned as ports 1-4) during recordings. Traditionally, SWRs are analytically determined by band-pass filtering at ripple frequency (ranging between 80-250 Hz) and considering any activity that exceeds the standard deviation (SD) of the mean to be a SWR (Csicsvari et al., 1999). For offline analysis, the mean is averaged across the whole session, and the SD is arbitrarily decided by the experimenter depending on the intended threshold sensitivity to SWR detection (3-5 SDs above the mean is common for defining SWRs). For real-time online detection of SWRs, the mean is a sliding average, and the SD threshold for the exponential moving average is set to 4. MATLAB is also used to help interface Xilinx with Cheetah as custom-generated SWR detection thresholds are inputted into MATLAB before each experimental recording to provide Xilinx parameters by which to scan for SWRs. These SWR detection thresholds were generated each day by taking a five-minute recording of the baseline LFP data and running it through another set of MATLAB code that will determine thresholds based on how close tetrodes are to the pyramidal cell layers, along with how prominently SWRs can be detected and analyzed. These thresholds were then directly inputted into MATLAB to provide Xilinx with accurate detection thresholds as it analyzed and scanned real-time LFP data for SWRs. Another component used in this setup is an Arduino board which controls the Master-8 Pulse Stimulator box to deliver current as our stimulation. Based on the location (CA1 or CA3) of the four tetrodes actively being surveyed by Xilinx, a specific Arduino function was selected for each experiment to customize the delivery of

the stimulus. For example, the experimenter can choose to have stimulations sent when SWRs are detected on ports that are recording SWRs observed in the CA1 or CA3 regions. In this example, a stimulation will be triggered upon detection of a SWR in either the CA1 region or the CA3 region. To test the general effects that electrical stimulation has on the brain without disrupting SWR events, 200 ms delays can also be incorporated. During these experiments, Xilinx will detect a SWR, but a stimulation will not be sent for an additional 200 ms, thus letting the SWR propagate uninterrupted. These experiments induce similar amounts of cellular inhibition without directly disrupting SWRs, and they will serve as direct controls to SWR disruption experiments. Single-pulses of bipolar current stimulation are generated by a Master-8 Pulse Stimulator box and sent into the animal's vHC region when commanded by the Arduino logic board. 200 ms lockout periods are always incorporated after each stimulation to help mitigate risk of seizure due to repetitive stimuli.

Offline Versus Online SWR Detection

Xilinx detection of SWRs in real-time is computationally heavy and inherently imperfect. Xilinx calculates SWRs in real-time by conducting an exponential moving average calculation of the bandpass-filtered (150-250 Hz) LFP data; any event that passes a threshold of four standard deviations above the mean neural activity is determined to be a SWR. Noise events cannot be excluded during real-time analysis and may be detected and stimulated upon. Additionally, other high-amplitude oscillations such as large DG spikes may also be incorrectly identified as a SWR and trigger stimulation. Overdetection/overstimulation is therefore common in most of these experiments. For these reasons, the efficiency of each experiment's SWR detection must be validated after each experiment by an offline analysis run through MATLAB that can determine "true" SWRs based on a very thorough analysis that excludes noise, DG spikes, and false events.

These “true” SWRs are represented by the orange circle in the figure 4 Venn diagram as the “offline SWR events.” Similar Venn Diagrams are generated after each experiment to show the overlap between the true number of SWRs that occurred during each trial block (offline SWR events) compared to the number of events that surpassed Xilinx SWR detection thresholds in real time (online SWR events). Higher overlap between the orange and blue circles indicates a higher percentage of the verified-true SWR events being stimulated upon during the live manipulation.

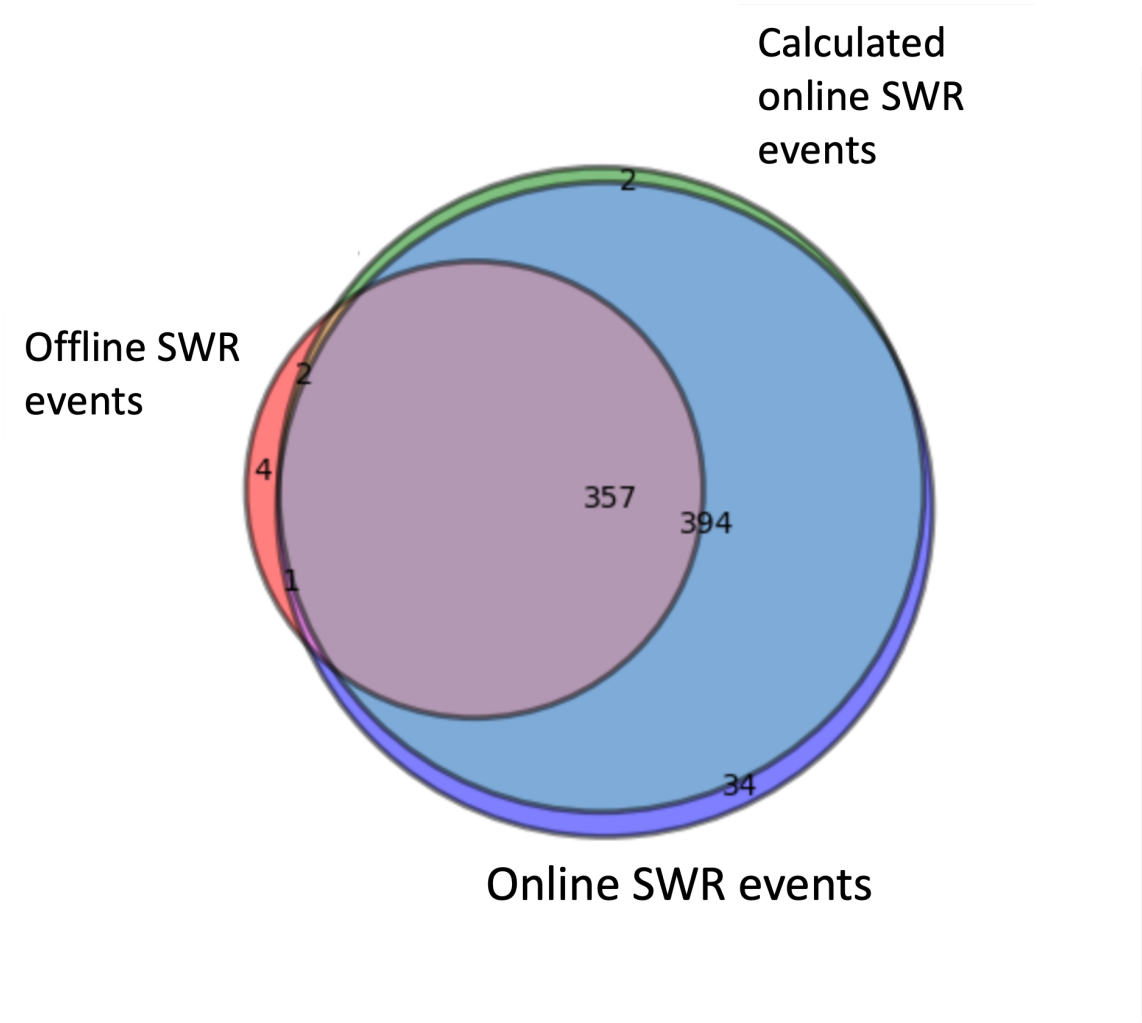

Figure 4. SWR Efficiency Was Assessed During NS Trials by Comparing SWRs Detected During the Experiment to an Offline Standard Algorithm. The orange "offline" circle represents the true number of SWR events that occurred during this example NS trial block. The blue "online" circle represents the number of events that surpassed SWR detection thresholds during the experiment. The green "calculated online" circle is determined by custom SWR detection thresholds generated before each experiment and serves as a guide for online SWR detection for Xilinx. The percentage of true "offline" SWR events that were disrupted during a given trial block can be calculated from the percentage of the orange offline circle that falls within the blue online detection circle. All Venn diagrams must be generated during no-stimulation trial blocks as verification of SWR accuracy would not be possible had stimulation been present.

Determination of Stimulation Strength

Once tetrodes have stabilized in the CA1 and CA3 layers, an input-output (I/O) curve is conducted to determine the appropriate stimulation strength needed to elicit the desired

inhibition. The experimenter begins by selecting a very low stimulation strength (generally 80-90 picoamps) and methodically increases it until clear changes can be seen on the hippocampal LFP following stimulation. Pyramidal neuron inhibition induced by vHC stimulation was assessed through the use of cross-correlation histogram plots (Figure 5A). The normal firing rate of a well-clustered pyramidal neuron was plotted over time with the stimulus artifact designated at time 0. Cellular inhibition can be assessed by measuring the length of time where the cell ceases to fire after the stimulus. Complete spiking silence of individual cells was analyzed; this approach was used for all cells previously determined to be pyramidal neurons. Previous literature (Jadhav et al., 2012) utilized a criteria of 100 ms of inhibition in CA1 neurons following stimulation, presumably because SWR events are typically ~100 ms in duration. For this reason, we decided to use the lowest stimulation strength that elicited roughly 100 ms of inhibition in CA1 pyramidal neurons to move forward with during experimentation. Stimulation strength and inhibition varied across animals; stimulation strengths anywhere from 100-180 pA induced a typical range of inhibition of 50-150 ms in CA1 or CA3 pyramidal neurons. The same stimulation strength was typically used across all experimental days for any given animal. A safety lockout of 200 ms was always incorporated after each stimulation during experimentation to reduce the potential for seizures.

Cellular Inhibition Induced by Bipolar Current Stimulation of the vHC

Two bipolar stimulating electrodes were implanted in the vHC region during surgery, one for each hemisphere (Figure 5B). Each bipolar electrode is made of two individual electrodes, allowing current to flow from the positive wire to the negative wire. The bipolar electrode with the best placement would be selected for experimentation moving forward. Although only one electrode was used for stimulation during experimentation, implantation of two bipolar

electrodes into the vHC region provided a fail-safe mechanism should one of the electrodes malfunction or not induce the desired hippocampal response. In addition, the contact of each pair of electrodes with the commissural fiber bundle greatly determines the effectiveness of stimulation and subsequent duration of inhibition. vHC stimulation led to the synchronous activation of a large number of principal cells and interneurons via the commissural fibers that connect CA3-CA3, CA3-DG, DG-DG (as well as CA3-CA1 via the Schaffer collaterals) across both hippocampal hemispheres (Girardeau et al., 2009). This activation burst was promptly followed by a rebounding inhibition effect that transiently silenced the hippocampal network (Girardeau et al., 2009). Stimulation was always triggered during experimentation upon Xilinx-mediated detection of SWR events in the CA1 or CA3 layers; ripples were subsequently disrupted roughly ~15-20 ms after detection (Figure 6).

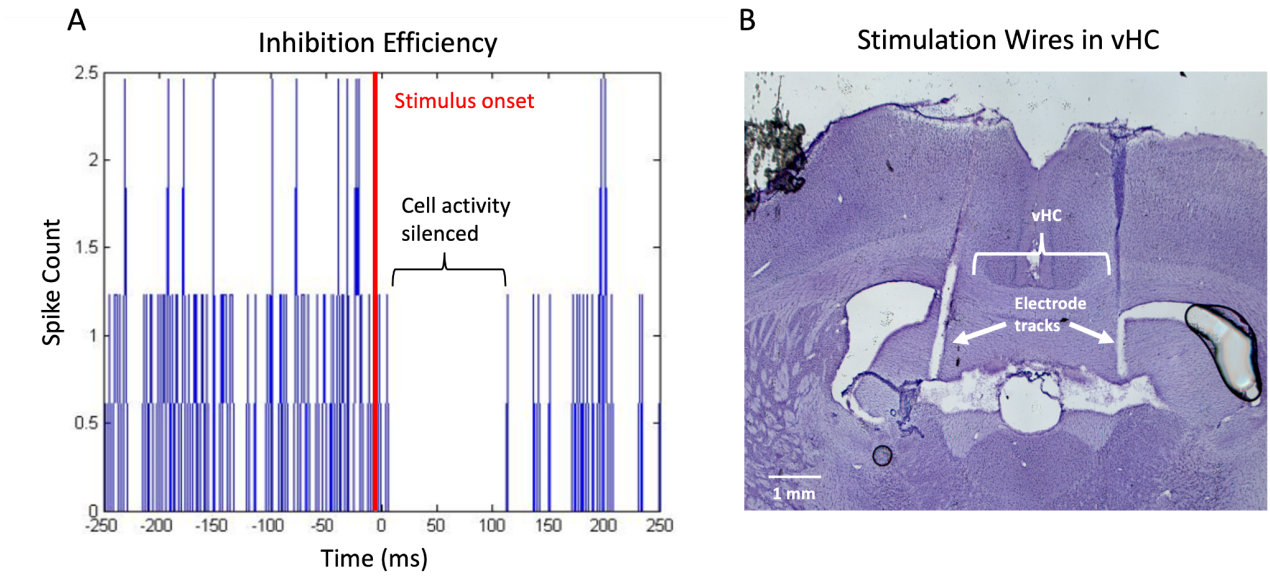

Figure 5. Inhibition Efficiency and Histological Visualization of Stimulation Wires in the vHC. A, The baseline firing rate of a CA3 pyramidal neuron was analyzed in relation to the stimulus artifact. Cellular inhibition was determined based on the length of spiking silence following the stimulus; this cell exhibited roughly 110 ms of inhibition following stimulation. **B**, Post-mortem confirmation of bilateral stimulation wires located in the vHC.

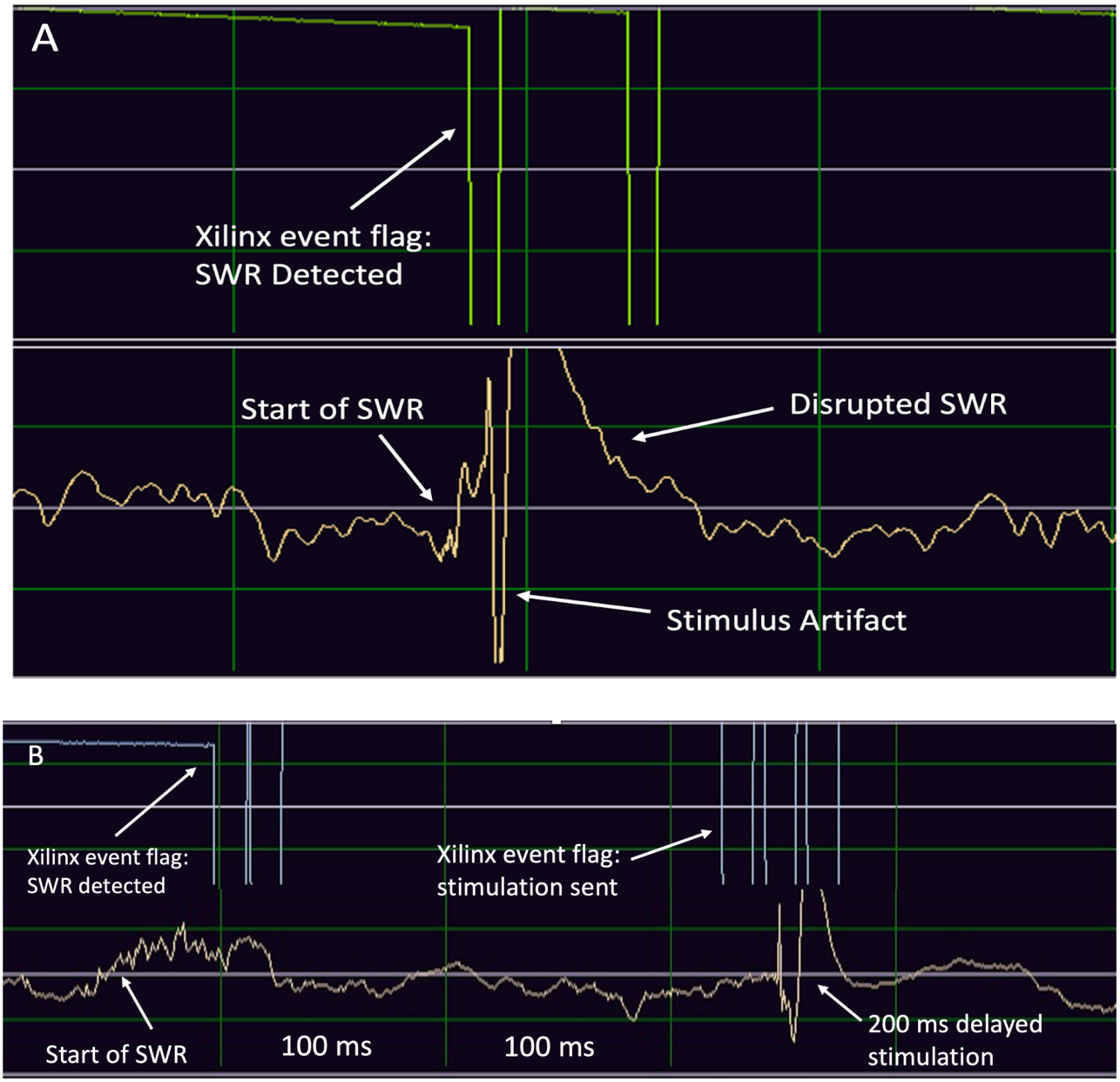

Figure 6. Xilinx Detection of SWR Triggers Stimulation and SWR Disruption. A, The top panel shows the event flags (these are digital indications that Xilinx is executing a command; 2 shown, one event flag indicated) generated when Xilinx detected a SWR on the specific port it was monitoring. Shortly after (~15 ms) the LFP pattern begins to change into the high-amplitude, high-frequency SWR event, a stimulation is sent into the vHC region to induce cellular inhibition and disrupt the SWR. **B,** SWR detection triggers 200 ms delayed stimulation.

Detection and Disruption of Hippocampal SWRs

In order to appropriately test the hypothesis that CA3 SWRs play a causal role in rodent spatial WM processes when DG input is required, simultaneous LFP recordings in the CA1 and CA3 subregions needed to be obtained. This combined LFP data is important for several reasons. First, it allowed for the duration of cellular inhibition induced in the CA1 versus the CA3 regions to be directly compared for each stimulation strength. A previous study by Jadhav et al. (2012) chose a 100 ms duration of inhibition in CA1 pyramidal neurons as their threshold for adequate SWR disruption; no such inhibition value has been proposed in the literature for CA3. Simultaneous recordings from the CA1 and CA3 regions will help shine light on the relationship between CA1 and CA3 inhibition caused by the vHC bipolar current stimulation technique. Additionally, disruption of SWRs observed in the CA1 region has been the standard method of disruption employed in previous literature (Girardeau et al., 2009; Jadhav et al., 2012). Finally, recent findings by Sasaki et al. (2018) show that CA3 SWR rates at 8-arm radial maze reward sites and during rest are suppressed without direct input from the DG. Combined CA1 and CA3 LFP recordings will allow us to seamlessly introduce a new manipulation (CA3 SWR disruption) alongside a familiar one that has been previously used (CA1 SWR disruption).

Two to three tetrodes were typically assigned to the CA1 region to record multiunit spike activity from CA1 pyramidal neurons in order to determine if adequate cellular inhibition was attained before SWR disruption experiments began. A majority of the remaining tetrodes would be indicated for the CA3 region, allowing us the chance to optimize recordings and simultaneously record the activity of a large population of cells. Tetrodes were chosen for either the CA1 or CA3 region based on their relative positions on the map of each hyperdrive. The final two tetrodes served as references: one remained higher up in the cortex to serve as a differential

reference electrode (R1), and the other served as a hippocampal reference for depth and general brain movement (R2). Due to our observation that CA1 SWRs did not always fire coherently with CA3 SWR events during behavior on the maze, tetrodes in the CA1 layer were also used to record and disrupt CA1 SWR events. It has been long stated in the literature that SWRs events are generated in the CA3 recurrent circuitry and propagate through the Schaffer collateral pathway to the CA1 layer where the SWR is visualized (Buzsáki, 2015). Our observations leave open the possibility that SWRs could be generated in both the CA3 and CA1 hippocampal subregions, or that all SWRs generated in CA3 may not propagate to CA1. Therefore, in order to most thoroughly assess if SWRs are mechanistically necessary for spatial WM processes, several experiments were performed where SWRs were disrupted in the CA1, CA3, and CA1 & CA3 regions.

Experimental Logic

The Arduino board commands the Master-8 box to send current delivery. Code written in the Arduino software can be customized to allow the experimenter to decide which detected SWRs will be allowed to result in the delivery of the stimulus. This is the "experimental logic," and it can be customized based on the intended type of experiment to be conducted each day. Most recording days contained tetrodes in both the CA1 and CA3 layers, allowing for various combinations of experiments. Considering that Xilinx only allowed for real-time SWR detection on four ports at once, the four tetrodes that had the most cells were chosen for live monitoring through Xilinx and Arduino. Arduino logic could be set to stimulate upon SWR detection in the CA1 region, CA3 region, or upon detection in either region at once (CA1 & CA3). Arduino code can also be customized to stimulate upon SWRs detected on any number of the four Xilinx ports, depending on which tetrode channels recorded the clearest LFP and spike activity, which

changes based on tetrode position and distance from the cellular layers. Additionally, 200 ms delays can be directly incorporated into the experimental logic through Arduino; these experiments serve as direct controls to the SWR disruption experiments as delayed-stimulation induced the same effects (cellular inhibition, LFP disruption) with the only exception being that SWRs were allowed to occur without disruption (Figure 6B).

Post-Mortem Histology

Upon completion of the final recording session, animals were prepared for euthanization. Animals were placed in a chamber and were incapacitated upon administration of 2.5-3.0% isoflurane gas with O_2. Sodium pentobarbital was injected intraperitoneally to induce euthanization. Pinch reflexes were confirmed to be absent prior to invasive perfusion methods. Intracardiac perfusion was performed with 200-300 mLs of phosphate buffered saline (PBS) followed by 200 mLs of 4% paraformaldehyde (PFA) in PBS (pH 7.4). Tetrodes were not removed from the brain for at least two hours following perfusion to aid in the reconstruction of tetrode tracks. Brains were extracted and submerged in 4% PFA overnight, then transferred to a 30% sucrose in PBS solution for another two to three days. Following equilibration in the sucrose solution, brains were then frozen and coronally sliced in 40 μm increments by a microtome. Relevant slices were then mounted on glass slides and left to dry overnight. Slides were then dehydrated using ethanol baths, stained with cresyl violet, and covered with coverslips. Once dry, slides were analyzed with a microscope to locate stimulation wires in the vHC and tetrode tracks in the hippocampus and surrounding cortical regions.

Tetrode Reconstruction

Following imaging, tetrode tracks were identified and tracked from entry to resting locations. Tracks were numerically ranked along the anterior-posterior axis, and tetrodes were

assigned to each track based on the map of the hyperdrive that was implanted on each animal and relative position of each tetrode in the tetrode bundle. Final resting locations included the CA1 cell layer, CA3 cell layer, DG, SR, or cortex (Figure 7). Stimulation wires were also confirmed to be positioned in the vHC (Figure 5B).

Statistical Analysis

A significance level of $\alpha = 0.05$ was used throughout this study. Any p-value < 0.05 was sufficient to reject the null hypothesis. Except for inhibition data ($n = 8$), data was averaged across nine animals used in this study. All data was first tested for normality using the Shapiro-Wilk test. Pearson R correlation calculations were performed to test if the slope of the linear regression trend lines were significant when data was normally distributed. If assumptions of normality were not met, then a Spearman's rank correlation was computed to test the strength of a monotonic relationship between the two variables. The Mann-Whitney U test was comprehensively used to scan for significant impairments in memory performance between and within experimental types. Due to the large number of tests performed, it was necessary to perform a Holm-Bonferroni test to correct for multiple comparisons. This test generated corrected p-values that were used to determine significance using the same significance level of $\alpha = 0.05$. Error bars on graphs indicate the standard deviation.

I would also like to acknowledge Yuhan Zhang for her computational support throughout this project. Her programs made it possible to detect and disrupt SWR events during the behavioral task. In addition to that, it was through her efforts that we were able to calculate the related SWR efficiency for all conducted experiments. I would also like to acknowledge Professor Stefan Leutgeb for his technical assistance throughout this project. Most notably, he

always conducted the lengthy surgical operations that were necessary to collect any of the data presented in this thesis.

This thesis is currently being prepared for submission of publication of the material by Zhang, Yuhan; Taylor, Brandon; Leutgeb, Stefan; Leutgeb, Jill. The author of this thesis will be a co-author of the publication.

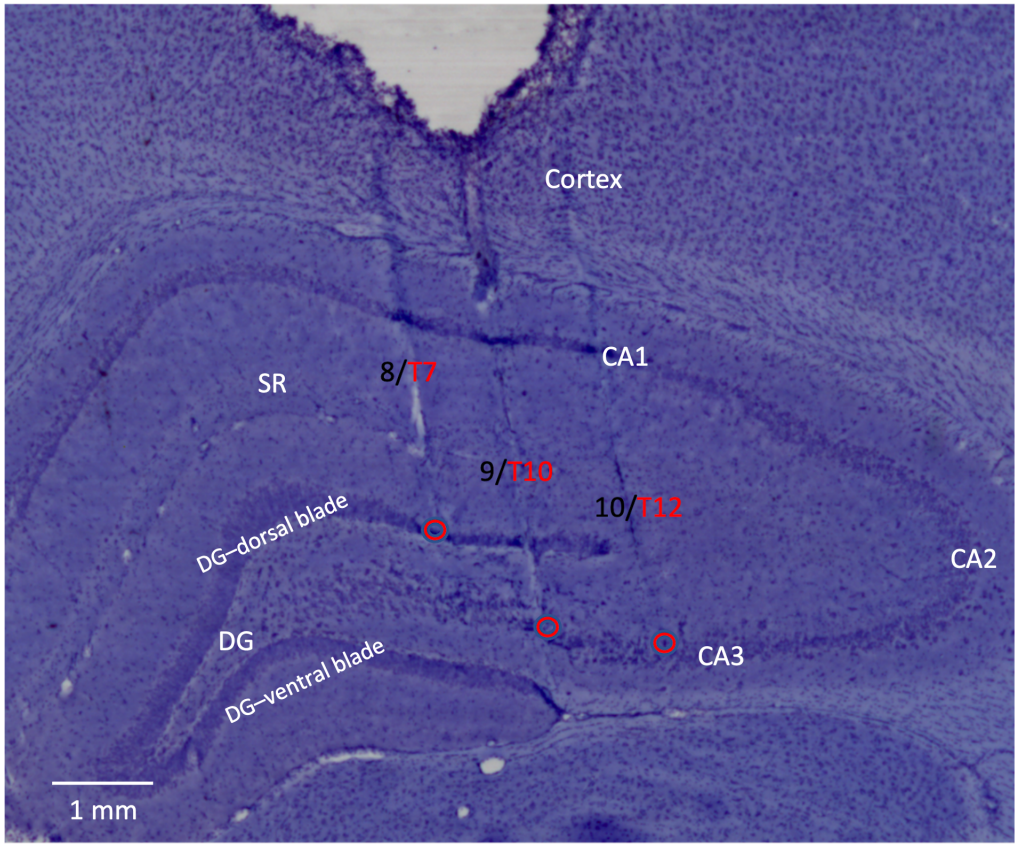

Figure 7. Tetrode Track Reconstruction. Final tetrode tracks were determined by histological visualization. Hyperdrive orientation, relative position in the tetrode bundle, and LFP data were all used to help infer which tracks matched with each tetrode. Tracks were numerically ranked in the order that they appeared on the anterior to posterior axis (black), and tetrodes (red text) were assigned to each track. Red circles indicate the approximate final resting location of each tetrode.

CHAPTER II – RESULTS

vHC Stimulation Induces Variable Inhibition in the CA1 and CA3 regions

Stimulation of the vHC region induces inhibition in pyramidal neurons that reside in the CA1 and CA3 regions. We always achieved 100 ms of inhibition in at least a couple CA1 cells by conducting an I/O curve before proceeding with a particular stimulation strength. Each data point that makes up figure 8 quantifies the mean length of inhibition obtained from all of the pyramidal neurons recorded from a given experiment. This included low-firing rate (LFR) and high-firing rate (HFR) pyramidal neurons, with exclusion of interneurons. This analysis revealed that average CA1 pyramidal neuron inhibition ($M = 85.6$, $SD = 56.0$) fell short of 100 ms in roughly 75% of the experiments conducted. Although CA3 inhibition was slightly less variable ($M = 78.4$, $SD = 30.4$), current literature does not discuss a threshold for CA3 inhibition that adequately disrupts SWRs. Figure 9 depicts the mean duration of inhibition in CA3 pyramidal neurons for each corresponding experiment containing simultaneously recorded CA1 cells that were inhibited. The CA1 data set was determined to be asymmetrically distributed using the Shapiro-Wilk test, $W(18) = .807$, $p = .002$, so a Spearman's rank correlation was computed to determine if a relationship between the duration of CA3 versus CA1 inhibition existed. There was a moderate positive correlation between the two variables, $r(19) = .55$, $p = 0.0047$, indicating that CA3 inhibition increased as a function of increasing CA1 inhibition. Several scatterplots were generated to assess if the duration of inhibition induced in CA1 or CA3 pyramidal neurons has any correlation with memory performance (measured in percent correct during stimulation trials) on the eight-arm radial maze. For all measured lengths of CA1 inhibition, memory performance during stimulation trials in SWR disruption experiments on the maze was not significantly impaired (Figure 10A), $r(15) = 0.13$, $p = 0.612$. Figure 10B also

includes each type of SWR stimulation experiment that was conducted based on the region that the SWR was detected in. The duration of inhibition obtained in our data is similar to previous studies that demonstrated impairments in memory consolidation and learning through the same SWR detection and stimulation manipulation (Girardeau et al., 2009; Jadhav et al., 2012), and the duration of inhibition matches the average length of a SWR observed on the LFP. These results indicate that duration of inhibition in CA1 pyramidal neurons is not correlated to memory performance on the spatial WM maze task.

We also sought to determine if inhibition of CA3 pyramidal neurons has any correlation with memory performance. Figure 11A is the CA3 companion to figure 10A, and it reveals that memory performance is not significantly correlated ($r(17) = -0.316$, $p = .188$) to any recorded duration of CA3 cellular inhibition induced during SWR disruption experiments. Figure 11B is the CA3 version of figure 10B; again the conclusion is that duration of CA3 inhibition is not associated with memory performance on the eight-arm radial maze under any of our experimental paradigms. In order to control for the relative inhibition efficiency and compare against previous inhibition thresholds of 100 ms in CA1 (Jadhav et al., 2012), we calculated for each experiment the percentage of CA1 cells that were inhibited at least 100 ms and compared this to memory performance on the radial maze during stimulation trials (Figure 12). This analysis indicates that, for all durations of inhibition that we induced in CA1 cells, memory performance on the eight-arm radial maze was not significantly impaired. Although a previous study by Jadhav et al. (2012) utilized an inhibition threshold of 100 ms in CA1 cells to ensure adequate disruption of neuronal activity during SWR events, our data indicates that this is not a hard threshold for inclusion. Figures 10 and 12 demonstrate that memory performance is not sensitive to the amount of inhibition induced in CA1 cells. Although an inhibition threshold has

never been discussed in the literature for CA3 cells, figure 11 also argues that memory performance during experiments is not correlated to the duration of CA3 inhibition. For these reasons, duration of inhibition was not used as a criterion for experiment inclusion.

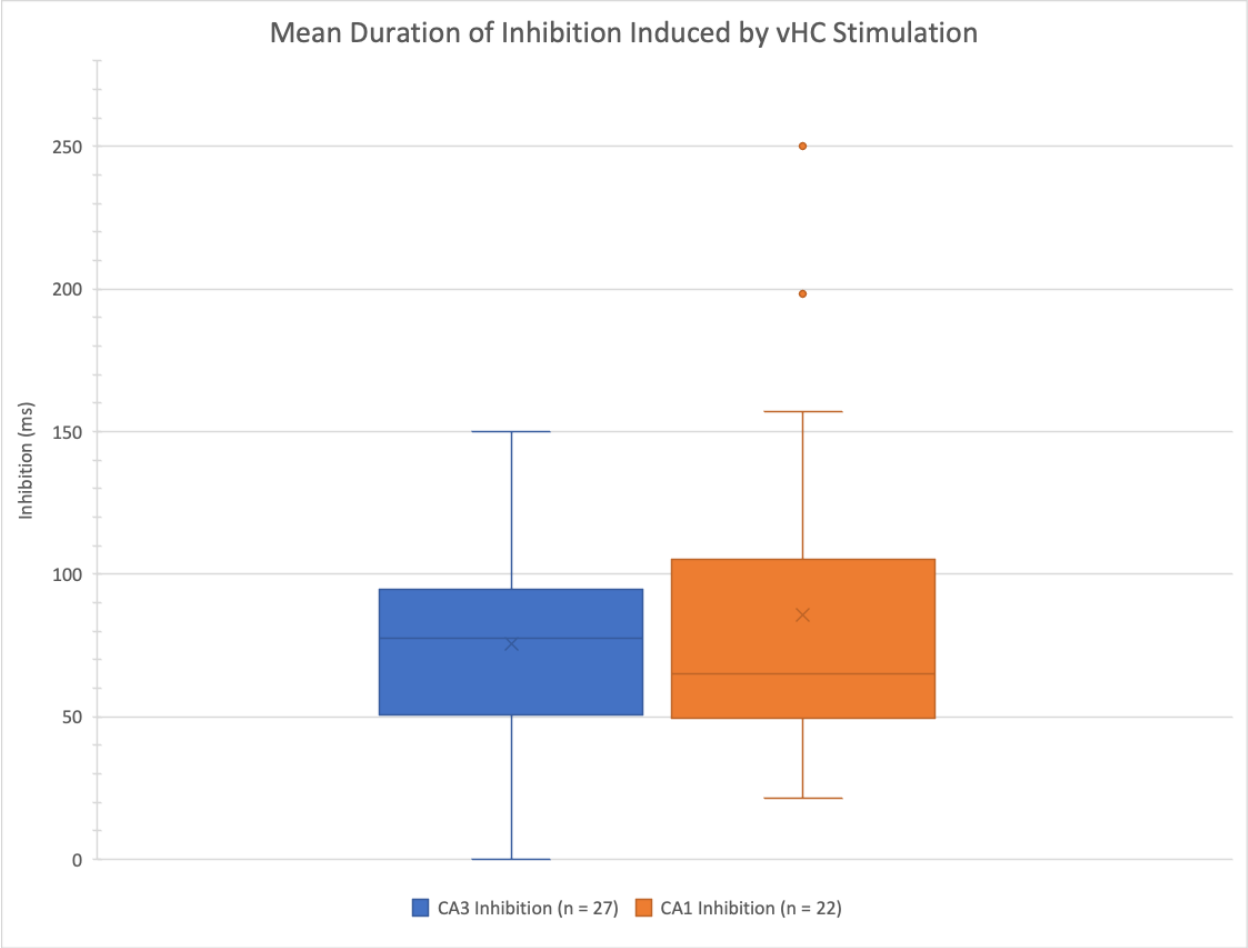

Figure 8. Mean Duration of Inhibition Induced in CA3 or CA1 Cells by vHC Stimulation. Box and whisker plot showing the relative levels of inhibition induced in either CA3 or CA1 pyramidal neurons. Each data point that was used to make this plot (n = 27 for CA3, n = 22 for CA1) represents the mean inhibition calculated from every recorded CA3 or CA1 pyramidal neuron that had an identifiable and isolatable spike cluster during any given experiment (i.e. the duration of inhibition for every cell in a single experiment is averaged into one number that represents one value for this plot). The "x" represents the mean inhibition of each data set.

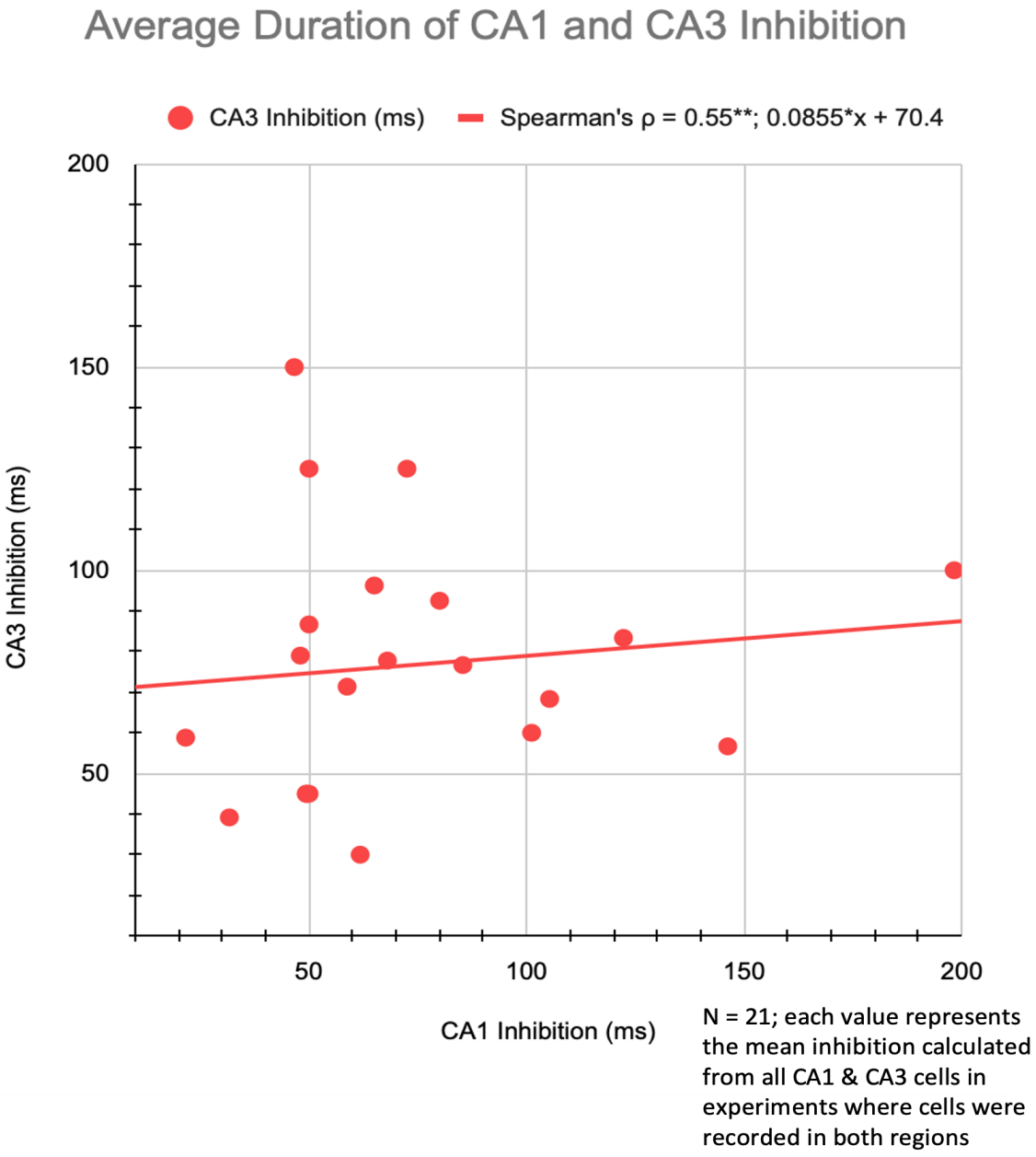

Figure 9. Relating Average Duration CA1 and CA3 Pyramidal Neuron Inhibition. Each data point represents the mean inhibition from all the CA3 or CA1 pyramidal cells for a given experiment. 21 experiments that contained measurable inhibition in both CA1 and CA3 pyramidal neurons were included in this analysis. A Spearman's rank correlation was computed to assess the relationship between the length of CA1 and CA3 inhibition. There was a moderate positive correlation between the two variables, $r(19) = .55$, $p = .0047$; this was significant at $\alpha = 0.05$. The red line represents the slope of a linear regression analysis.

Figure 10. Memory Performance Relative to Mean Duration of CA1 Pyramidal Neuron Inhibition. A, Each data point represents the mean duration of inhibition calculated from the total number of well-defined CA1 pyramidal neurons recorded on all tetrodes near the CA1 layer during any given experiment. % correct (Stimulation trials) represents the mean memory performance averaged across all stimulation trials for a given experiment. A Spearman's rank correlation was computed to assess the relationship between the length of CA1 inhibition and memory performance on the maze during stimulation trials. There was no detected relationship between the two variables, $r(15) = 0.13$, $p = 0.612$. The red trend line represents the slope of a linear regression analysis. **B,** CA1 inhibition versus memory performance for each type of SWR experiment conducted. SWR D&S refers to region-specific SWR detection and subsequent vHC stimulation. Red icons represent experiments where SWR detection in the CA3, CA1 & CA3, or CA1 regions triggered the exact same vHC stimulation designed to disrupt SWR-associated neuronal activity. Blue 200 ms delay experiments incorporate a waiting period of 200 ms to pass after SWRs are detected in the appropriate region before stimulations are sent into the vHC region. Although the cellular inhibition induced in these delay experiments does not occur during SWRs, they have been included in the graph for comparison to show memory performance for those groups.

A

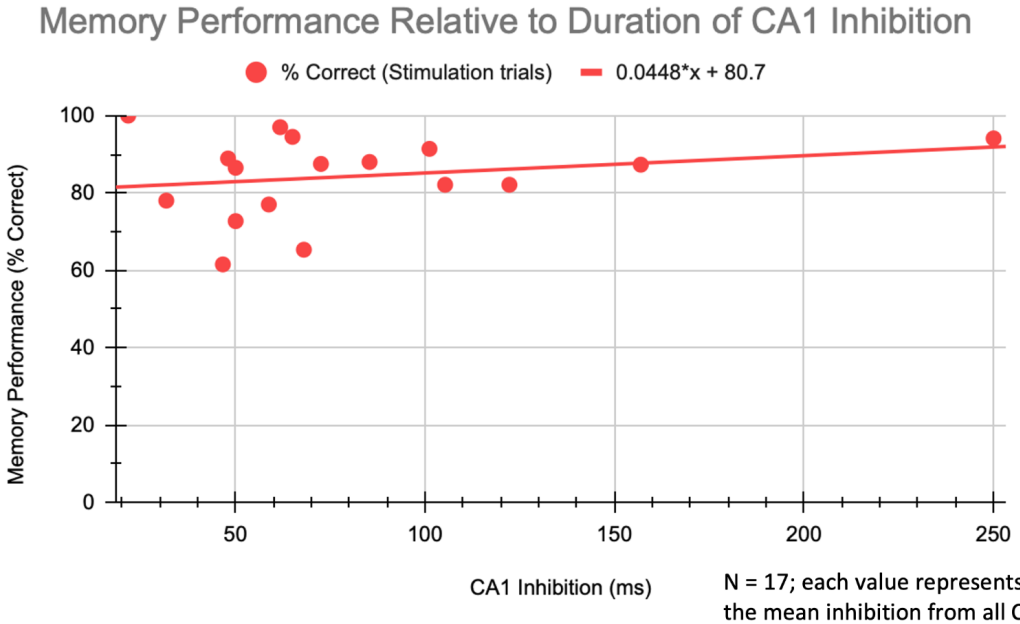

N = 17; each value represents the mean inhibition from all CA1 cells for any SWR disruption experiment

B

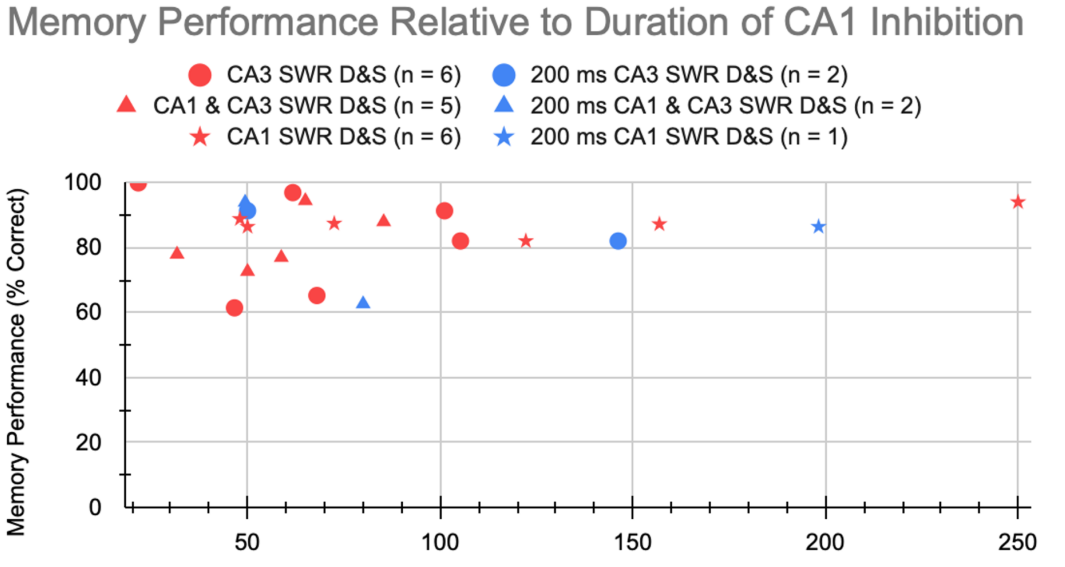

D&S = SWR Detection & vHC Stimulation

N = 22; each value represents the mean inhibition from all CA1 cells for any given experiment

Figure 11. Memory Performance Relative to Mean Duration of CA3 Pyramidal Neuron Inhibition. A, Each data point represents the mean inhibition from all the CA3 pyramidal cells recorded during any given experiment. The red trend line represents the slope of a linear regression analysis. CA3 inhibition was confirmed to be normally distributed (Spapiro-Wilk test). There was a weak, negative correlation between the two variables, $r(17) = -0.316$, $p = 0.188$; however, the relationship was not significant at $\alpha = 0.05$. **B,** CA3 inhibition versus memory performance for each type of SWR experiment conducted. SWR D&S refers to region-specific SWR detection and subsequent vHC stimulation. Red icons represent experiments where SWR detection in the CA3, CA1 & CA3, or CA1 regions triggered the exact same vHC stimulation designed to disrupt SWR-associated neuronal activity. Blue 200 ms delay experiments incorporate a waiting period of 200 ms to pass after SWRs are detected in the appropriate region before stimulations are sent into the vHC region. Although the cellular inhibition induced in these delay experiments does not occur during SWRs, they have been included in the graph for comparison to show memory performance for those groups.

A

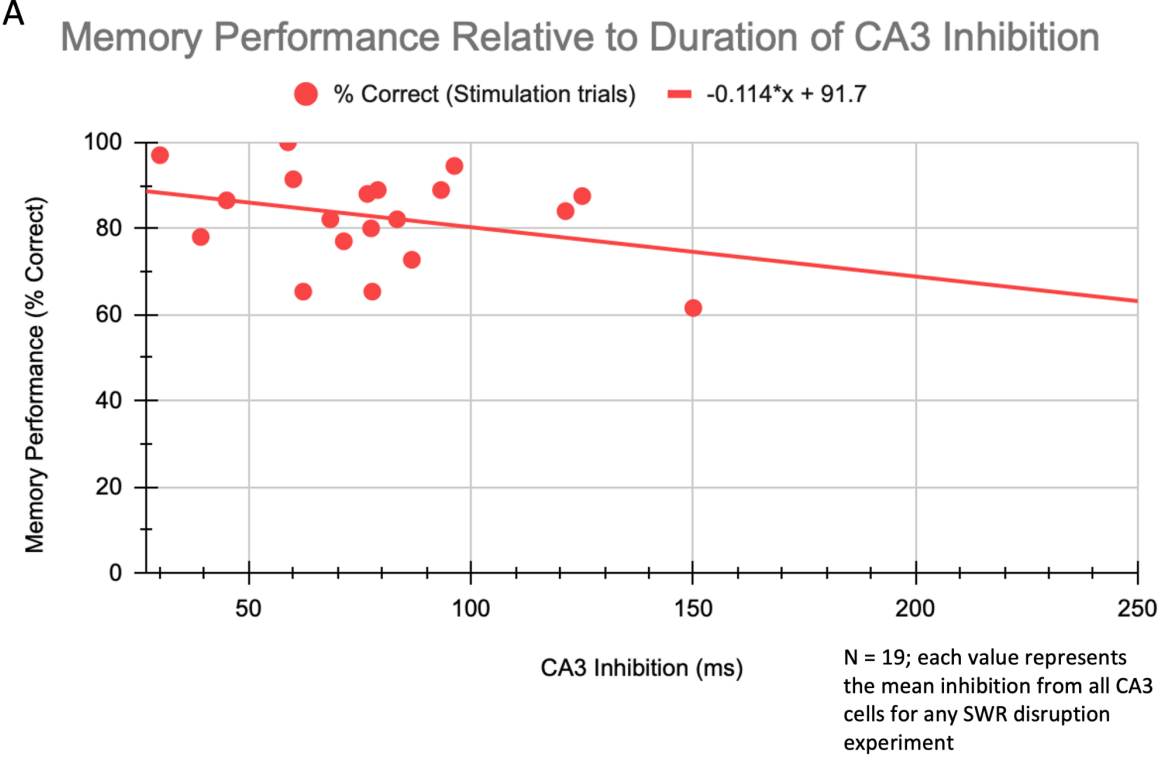

N = 19; each value represents the mean inhibition from all CA3 cells for any SWR disruption experiment

B

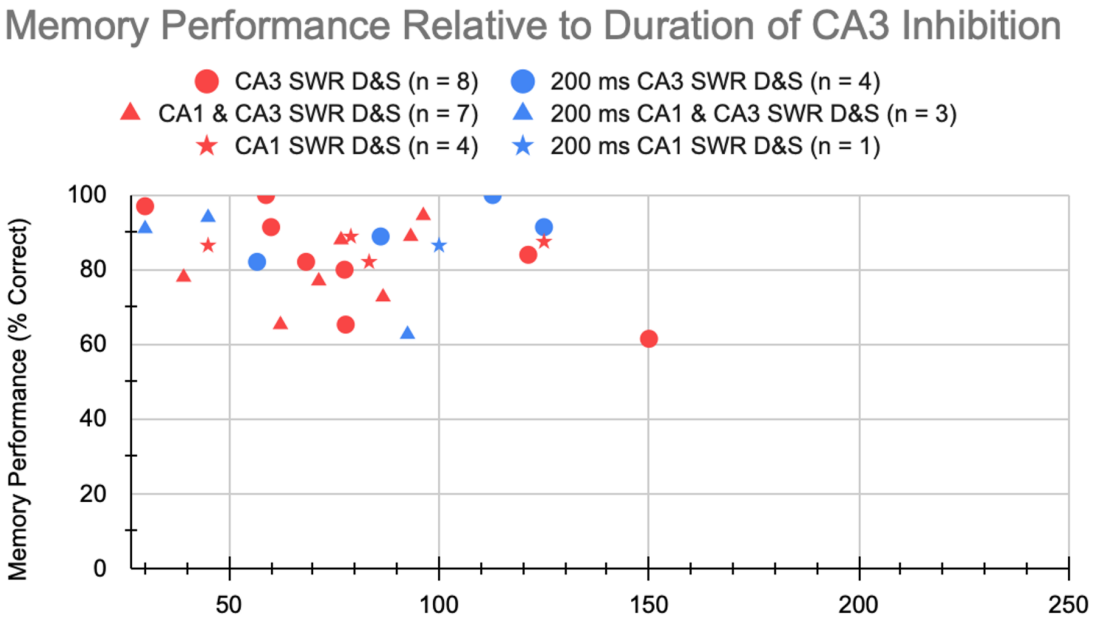

D&S = SWR Detection & vHC Stimulation

N = 27; each value represents the mean inhibition from all CA3 cells for any given experiment

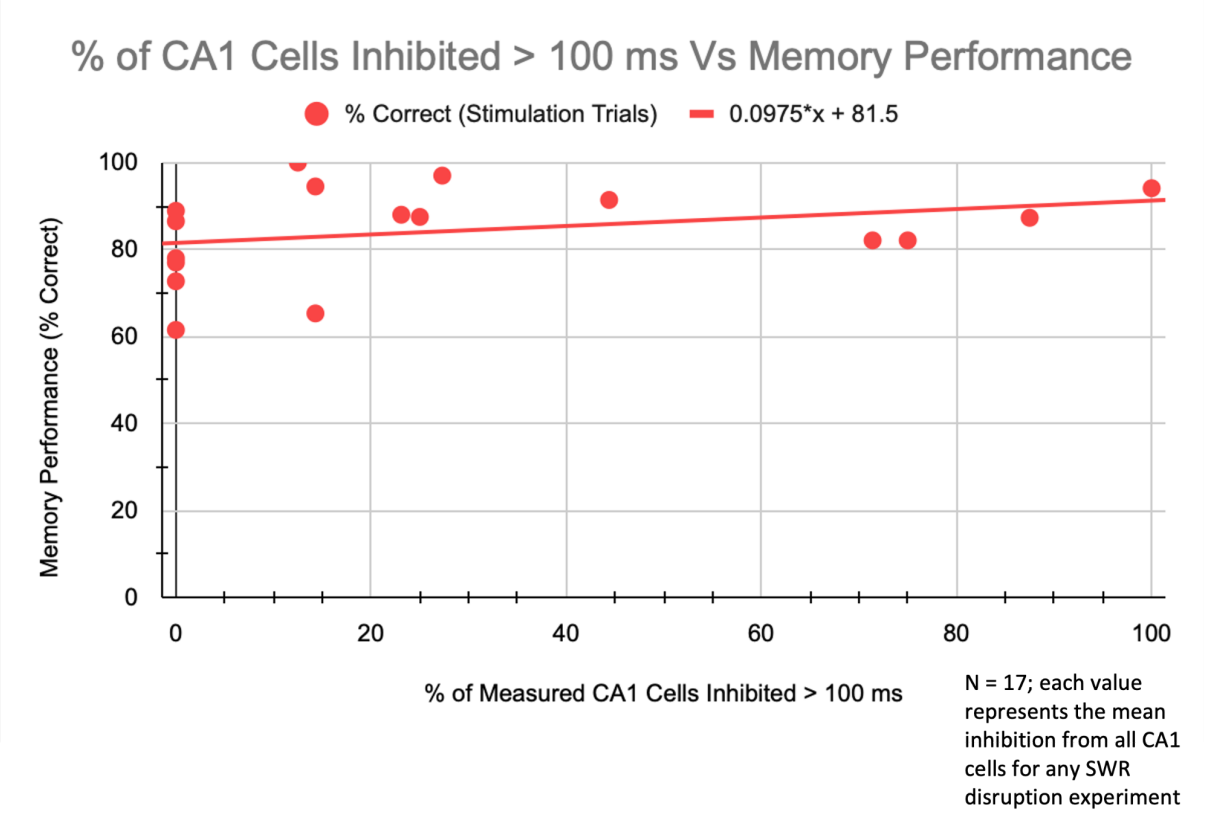

Figure 12. Percentage of CA1 Cells Inhibited > 100 ms Versus Memory Performance. The percentage of CA1 cells that were inhibited over 100 ms was calculated for each SWR disruption experiment that contained CA1 cells with measurable inhibition. There was no detected correlation between the two variables, $r(15) = .309$, $p = .228$.

Increased SWR Detection Efficiency Does Not Impair Spatial WM Performance

Considering that duration of inhibition in CA1 and CA3 pyramidal cells is decoupled with memory performance on the 8-arm radial maze spatial WM task, we will now consider the role that SWR disruption has on memory performance. Venn diagrams such as the example in figure 4 allowed us to calculate the SWR detection accuracy during experiments in order to exclude instances where SWR detection was not optimal. Figure 13 plots the SWR detection efficiency against average memory performance during stimulation and no-stimulation trials for 27 SWR disruption experiments. Increasing the percentage of SWRs that were detected and

disrupted during any given experiment does not impair memory performance on the 8-arm radial maze spatial WM task.

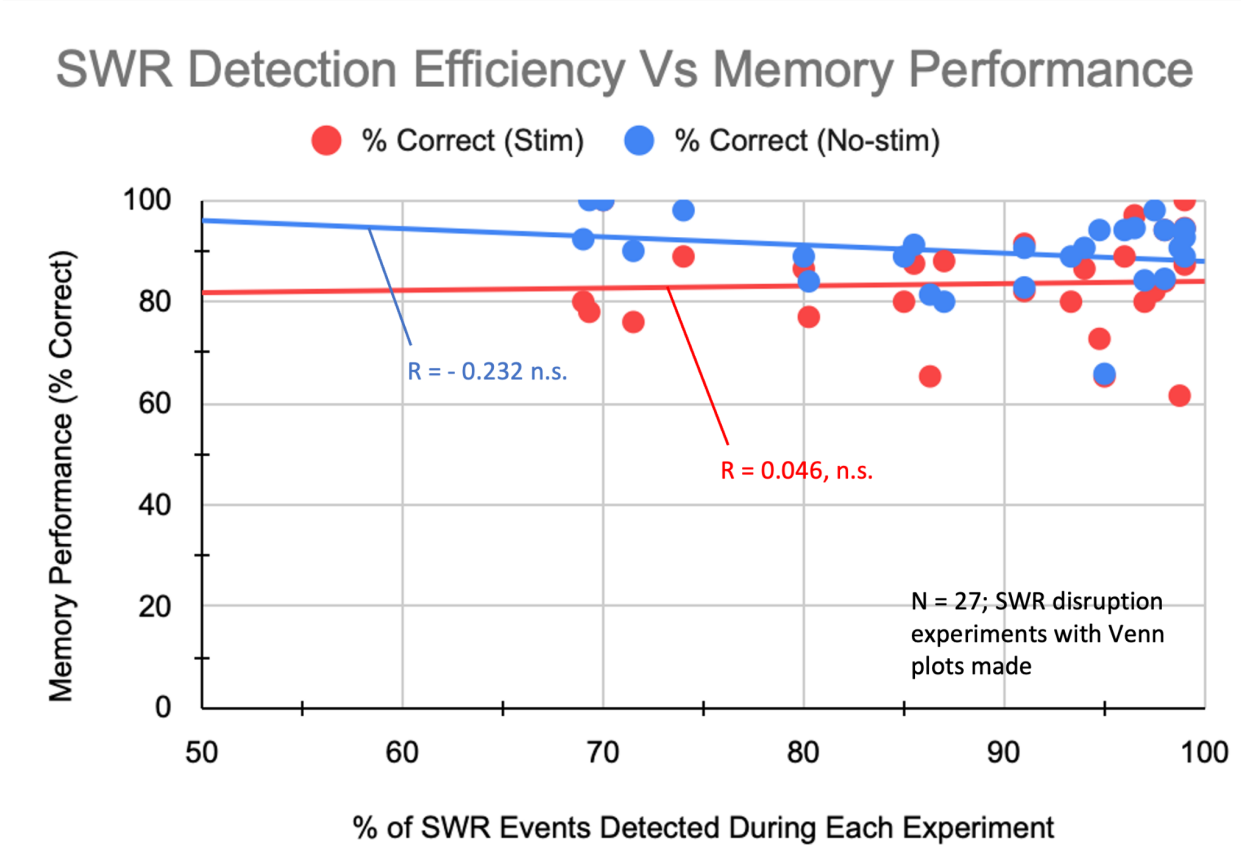

Figure 13. SWR Detection Efficiency Versus Memory Performance. The percentage of SWR events detected was plotted against average memory performance for all stimulation and no-stimulation trials for a total of 27 SWR disruption experiments; each dot represents the average % correct for all trials within one experiment. Only SWRs detected during "stim" trials triggered stimulation of the vHC region. The slope of both linear trend lines is not significant; r(25) = -.232, p = .246 (blue, no-stim line), r(25) = .046, p = .819 (red, stim line).

SWR Disruption Does Not Impair Spatial WM Memory Performance

Increased detection and disruption of SWRs is not correlated with memory performance on the maze. We will now shift the focus to analyze SWR disruption on a temporal basis throughout each experiment. Trial blocks (NS1, S1, etc.) were compared to one another for each type of SWR detection experiment to assess if any temporal impairments in memory

performance could be induced by SWR disruption. Figure 14A demonstrates how trial blocks incorporating stimulation after SWR detection introduce more variability in the animal's performance on the maze. Interestingly, this variability and deviance (measured in % correct) lessen over time as the experiment proceeds. Comprehensive application of the Mann-Whitney U test initially reported statistically significant differences in memory performance on the maze in the SWR disruption group between S1 and NS3 trial blocks ($N = 20$, $U = 108.5$, $Z = -2.32$, $p = 0.021$), as well as S2 and NS3 ($N = 20$, $U = 117$, $Z = -2.07$, $p = 0.038$), refer to figure 14A, table 1B. To account for the multiple comparisons conducted, a Holm-Bonferroni correction (H-Bc) was applied. After Holm-Bonferroni correction, no significant temporal differences in memory performance were detected for the SWR disruption group (H-Bc α for $p = 0.021$ is .00094, $0.021 > .00094$, N.S.); (H-Bc α for $p = 0.038$ is .00096, $0.038 > .00096$, N.S.), (Table 1B, "within differences"), indicating these previous results were obtained purely by chance. No significant differences in memory performance were found between any of the SWR disruption groups and their corresponding 200 ms delay experiments (Table 1A, "between" differences). Figure 14B further classifies experiments into different categories based on the unique SWR detection logic utilized. Initially, significant differences were found in the CA1 SWR disruption experiments between NS1 and NS3 trial blocks ($N = 5$, $U = 1$, $Z = -2.36$, $p = .0184$), S1 and NS3 ($N = 5$, $U = 1$, $Z = -2.39$, $p = .0172$), as well as in the CA1 & CA3 disruption experiment between NS2 and S2 ($N = 5$, $U = 23.5$, $Z = 2.21$, $p = .027$) after comprehensive Mann-U Whitney testing. All other relationships within and between experiments proved to be insignificant. After Holm-Bonferroni correction, no significant temporal differences in memory performance were detected for the any of the aforementioned groups (H-Bc α for $p = 0.018$ is .00091, $0.018 > .00091$, N.S.); (H-Bc α for $p = 0.017$ is .00089, $0.017 > .00089$, N.S.), (H-Bc α for $p = 0.027$ is .00094, $0.027 > .00094$,

N.S.), (Table 1B, “within differences”), again indicating these initially significant results were obtained by chance. Similar to before, no significant differences in memory performance were found between any of the SWR disruption groups and their corresponding 200 ms delay experiments (Table 1A, “between” differences). The relative lack of impairment in spatial WM performance during situations where SWRs are disrupted implies SWRs are not mechanistically important for spatial WM processes.

Figure 14. Memory Performance Across Trial Blocks Compared Between Disruption and Control Experiments. A, Memory performance was temporally compared among trial blocks between SWR disruption experiments (red) and 200 ms control experiments (blue). All included experiments were selected if they had a SWR detection efficiency ≥ 85%. The x-axis represents trial blocks during an experiment (groups of 4 consecutive trials); NS1 = first set of no-stimulation trials (1-4), S1 = first set of stimulation trials (5-8), and so forth. All possible combinations were statistically compared "within" the experiment (between pairs of trial blocks) and "between" experiments (disruption vs 200 ms delay controls) using a Mann-Whitney U test (view table 1). No significant differences in memory performance were detected "within" or "between" any of the experiments after Holm-Bonferroni correction. Error bars on graphs indicate standard deviation. **B,** Additional data was included for each type of SWR experiment conducted. 200 ms CA1 controls were excluded from the plot as the sample size was n = 1. No significant differences in memory performance were detected "within" or "between" any of the experiments after Holm-Bonferroni correction.

A

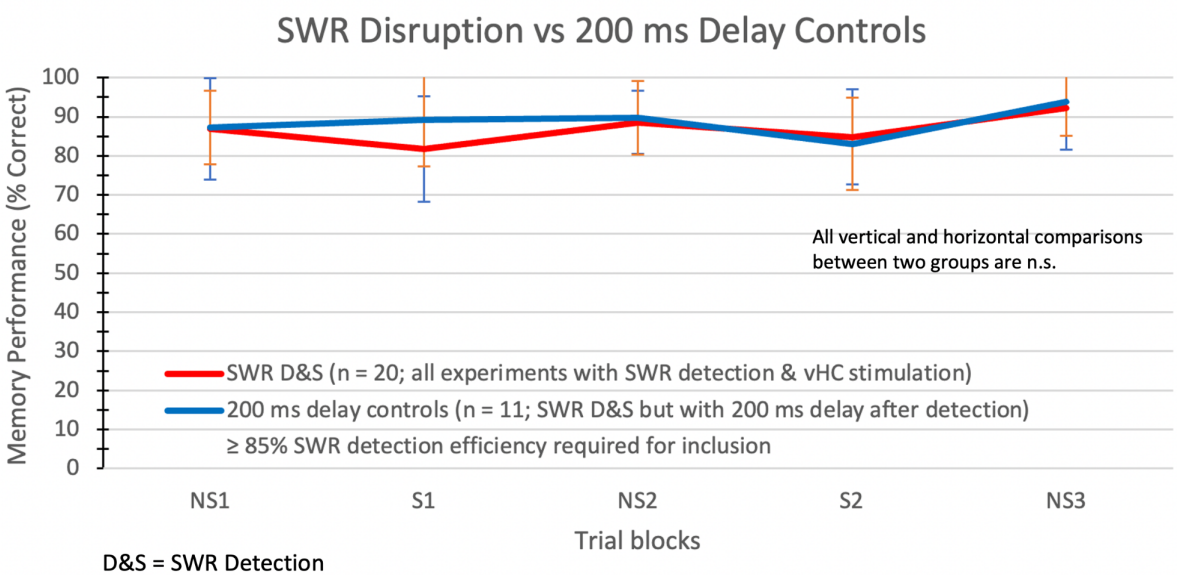

D&S = SWR Detection & vHC Stimulation

B

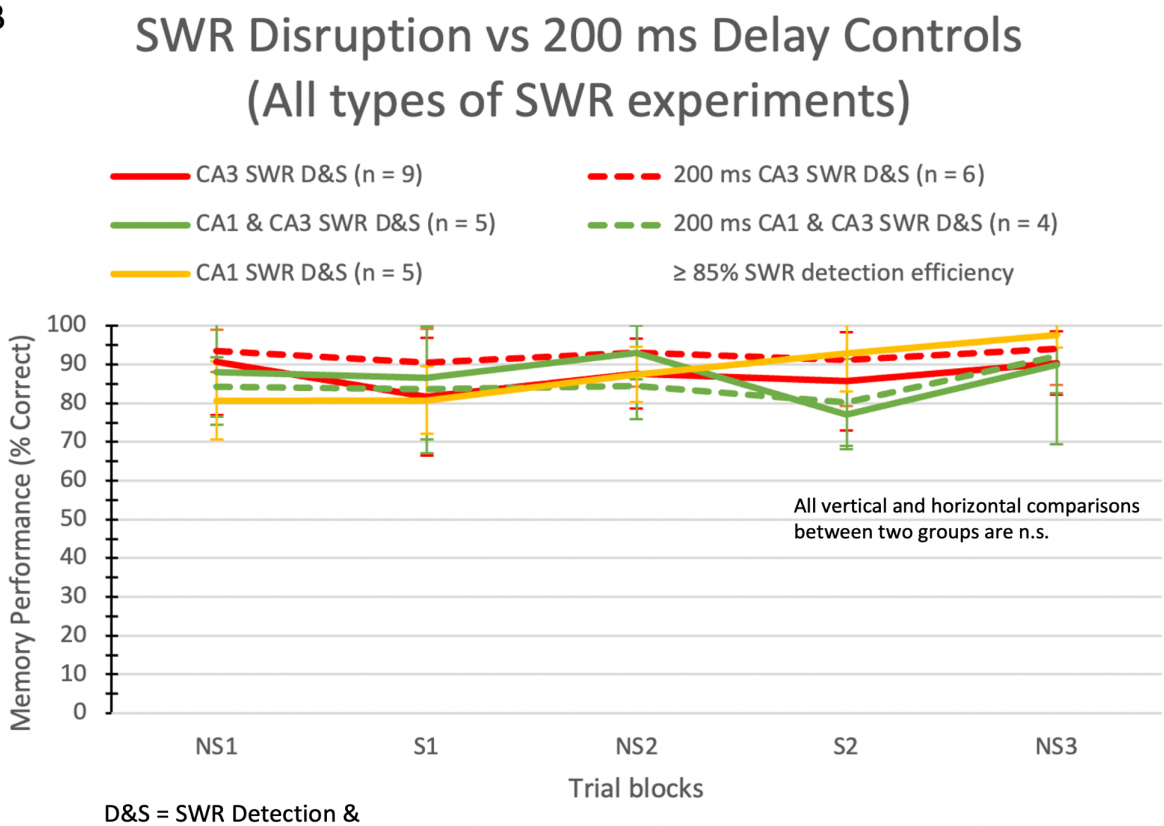

D&S = SWR Detection & vHC Stimulation

Table 1. Mann-Whitney U Test P-values For Analysis of "Within" and "Between" Experimental Controls. A, Calculated p-values ($\alpha = 0.05$) for the "between" experimental comparisons. All SWR disruption experiments' trial blocks were directly compared to their corresponding 200 ms control experiment; i.e. NS1 for CA3 SWR disruption was directly compared to NS1 for 200 ms delay control CA3 experiments. Identical p-values for paired groups were left in the table to allow easy determination of groups being directly compared. No significant differences were detected among any of the groups using a Mann-Whitney U test after Holm-Bonferroni correction. **B,** Calculated p-values for the "within" experimental controls. Trial blocks (NS1, S1, etc.) were compared to one another for each type of SWR detection experiment. Although **five*** significant differences were found upon initial application of the Mann-Whitney U test, these p-values did not reach significance after Holm-Bonferroni correction.

Table 1A "Between"	All SWR disruption (N=20)	All SWR 200 ms controls (N = 11)	CA3 SWR Disruption (N = 10)	200 ms CA3 SWR (N = 6)	CA1 & CA3 SWR Disruption (N =5)	200 ms CA1 & CA3 SWR (N = 4)	CA1 SWR Disruption (N = 5)	200 ms CA1 SWR (N = 1)	Holm-Bonferroni Correction (H-Bc)
NS1 vs NS1	0.851	0.851	1	1	0.537	0.537	0.373	0.373	N.S.
S1 vs S1	0.182	0.182	0.664	0.664	0.621	0.621	0.213	0.213	N.S.
NS2 vs NS2	0.573	0.573	0.297	0.297	0.176	0.176	0.228	0.228	N.S.
S2 vs S2	0.983	0.983	0.349	0.349	0.797	0.797	0.546	0.546	N.S.
NS3 vs NS3	0.596	0.596	0.372	0.372	0.869	0.869	0.724	0.724	N.S.

Table 1B "Within"	All SWR disruption (N=20)	All SWR 200 ms controls (N = 11)	CA3 SWR Disruption (N = 10)	200 ms CA3 SWR (N = 6)	CA1 & CA3 SWR Disruption (N =5)	200 ms CA1 & CA3 SWR (N = 4)	CA1 SWR Disruption (N = 5)	200 ms CA1 SWR (N = 1)	Holm-Bonferroni Correction (H-Bc)
NS1 vs S1	0.198	0.739	0.106	0.51	1	0.46	0.914	n too small	N.S.
NS1 vs NS2	0.88	0.331	0.265	0.738	0.664	0.882	0.284	n too small	N.S.
NS1 vs S2	0.397	0.764	0.133	1	0.171	0.661	0.09	n too small	N.S.

Table 1. Mann-Whitney U Test P-values For Analysis of "Within" and "Between" Experimental Controls, Continued.

NS1 vs NS3	0.254	0.159	0.417	0.796	0.687	0.297	**0.018***	n too small	*After H-Bc: α =.00091 **N.S.** (0.018 > .00091)
S1 vs S2	0.487	0.526	0.47	0.933	0.401	0.77	0.133	n too small	N.S.
S1 vs NS3	**0.021***	0.269	0.223	0.49	0.687	0.559	**0.017***	n too small	*After H-Bc: α =.00089, .00093 **N.S.** (0.017 > .00089), (0.021 > .00093)
NS2 vs S2	0.421	0.44	0.939	1	**0.027***	0.657	0.278	n too small	*After H-Bc: α = .00094 **N.S.** (0.027 > .00094)
S2 vs NS3	**0.038***	0.075	0.421	0.591	0.26	0.18	0.488	n too small	*After H-Bc: α = .00096 **N.S.** (0.038 > .00096)

CHAPTER III – DISCUSSION

SWRs are generated by the recurrent CA3 circuitry and are observed in the CA1 region of the mammalian hippocampus (Buzsáki, 2015). SWRs occur while the brain is in an offline state, such as during periods of non-REM sleep, immobility, and consummatory behaviors (Joo & Frank, 2018). Previous literature has highlighted many functional roles for the SWR as it relates to numerous phases of memory formation. Fundamentally, the SWR is best characterized by the excitatory population burst of pyramidal neurons in the CA3 region. Considering how SWR events also drive the simultaneous activation of surrounding cortical regions (Wierzynski et al., 2009), and coincident depolarization between neurons can facilitate LTP induction (Whitlock et al., 2006), the SWR is a perfect candidate for a hippocampal oscillation that can mediate numerous crucial memory processes simultaneously. Upon closer analysis, researchers have discovered that there is a temporal association between the large number of neurons that are simultaneously excited. Nádasdy et al. (1999) first reported that SWRs synchronize the time-compressed reactivation of place cells in a sequential and ordered manner. Later research by Foster & Wilson (2006) would expand upon these findings by revealing that SWRs facilitate the reversed replay of place cells after behavior, potentially serving as a mechanism to consolidate the path taken to the recently-retrieved reward. Conversely, forward replay events have also been observed to activate place cells that depict spatial trajectories towards upcoming goal locations (Pfeiffer & Foster, 2013). These findings motivated a whole field of research that investigates the potential role that the SWR plays in guiding memory during ongoing behavior. Considering the large body of literature that has identified the functional DG to be necessary for spatial WM tasks (McLamb et al., 1988; McNaughton et al., 1989; Walsh et al., 1986, as cited in Xavier & Costa, 2009), Sasaki et al. (2018) analyzed CA3 SWR activity with and without functional DG

inputs. CA3 place cells containing place fields for future reward arms were preferentially activated during CA3 SWR events after reward consumption. Lesions to the DG greatly attenuated CA3 SWR activity, even impairing the activation of CA3 place cells that represented future goal locations on the 8-arm radial maze, supporting previous findings by Pfeiffer & Foster (2013). Animals with these DG lesions performed drastically worse than control animals on the spatial WM radial maze, leading the team to conclude that the CA3 SWRs may be mechanistically supporting spatial WM processes (Sasaki et al., 2018). The growing evidence led researchers to hypothesize that online SWRs were necessary for guiding upcoming decision making in spatial WM tasks, although the mechanism remained unknown and had yet to be causally tested.

Several methods have been developed to disrupt SWR activity, including tet-x inducible blockade at the CA3-CA1 synapse using transgenic mice (Nakashiba et al., 2009), high-frequency optogenetic stimulation of the locus coeruleus after SWRs during sleep (Novitskaya et al., 2016), and electrical disruption of ripples through vHC stimulation (Girardeau et al., 2009; Jadhav et al., 2012). Depending on the specific methods and time of disruption, SWR disruption can cause impairments in consolidation, retrieval, learning, and various types of memory. Previously, Jadhav et al. (2012) demonstrated that electrical disruption of CA1 SWRs through vHC stimulation during awake behavior disrupts learning on the outbound, but not inbound, component of a spatial alternation W-track maze task. The outbound component requires the animal to make a left-or-right decision about where to turn next to retrieve the next reward on the maze, hence why it is considered to be the memory-guided decision making portion of the maze (Jadhav et al., 2012). This is in contrast to the inbound component of the maze, which tests reference memory, which is the ability to return to previously visited locations.

Although these findings highlight a role for CA1 SWRs in learning processes, the study was not designed to test the role that SWRs play in spatial WM. The spatial alternation task chosen in this study fails to provide the robust statistical error analysis needed to analyze the role SWRs play in ongoing spatial WM as there was a 50% chance of the rat making the correct choice (left arm or right arm) on each outbound choice. In order to test the specific role that SWRs play in spatial WM tasks, a study must be conducted that disrupts SWRs while they occur in real time during a complex spatial WM task. For this reason, we decided to test rats' spatial WM performance on the 8-arm radial maze task; this will allow us more power in our statistical analysis and thus more confidence that we are truly observing the intended results of our manipulation while minimizing confounding variables. In our current study, we attempted to disrupt SWR events in the CA3, CA1, or CA1 & CA3 regions while rats traversed the dentate-dependent 8-arm radial maze (Sasaki et al., 2018) to assess if CA3 SWRs are causally linked to spatial WM processes. We detected SWRs in the CA3, CA1, or CA1 & CA3 hippocampal subregions using an online detection algorithm that uses custom SWR detection thresholds that were decided on prior to each experiment based on the relative position of each tetrode near the cell layers. When SWRs were detected, electrical stimulation of the vHC fibers was initiated, resulting in a transient silencing of hippocampal pyramidal neurons and subsequent SWR disruption. This online vHC stimulation protocol matched what was used in previous studies (Girardeau et al., 2009; Jadhav et al., 2012), and it is favorable to other SWR disruption techniques because it induces maximal transient cellular inhibition in the hippocampus on a tight temporal timeframe. 200 ms delay control experiments had similar levels of cellular inhibition and stimulation frequency, but they differed from disruption experiments because SWRs were allowed to propagate unablated before stimulation occurred shortly after. Inhibition and SWR

detection/disruption efficiency was analyzed after each experiment to validate the experimental success. Using this experimental paradigm, we were able to directly test our hypothesis that CA3 SWRs play a necessary role in spatial WM processes on a dentate-dependent spatial WM task.

In order to effectively disrupt and truncate SWR events in the different hippocampal subregions, we first needed to assess the efficacy of our inhibition protocol by measuring the duration of CA1 and CA3 pyramidal neuron spiking silence after stimulation to the vHC region. A previous study by Jadhav et al. (2012) decided to use experiments that elicited ~100 ms of inhibition in CA1 pyramidal neurons. Since they were the first group to demonstrate that disruption of awake SWRs impairs learning, they also had to arbitrarily decide on an inhibition threshold. They arbitrarily settled on this threshold by choosing a stimulation strength that inhibited the multiunit spike activity for ~100 ms. Girardeau et al. (2009) previously used the same vHC stimulation method to transiently disrupt SWR activity during post-training sleep, although they used stimulation strengths that resulted in less than 100 ms of CA1 inhibition so they could induce "selective and transient perturbation of the hippocampal network activity." For these reasons, we also decided to aim for 100 ms of inhibition in CA1 pyramidal neurons after vHC stimulation. Input/output (I/O) curves were always conducted before experimental manipulation for each animal to determine sufficient stimulation strengths to elicit ~100 ms of inhibition in CA1 pyramidal neurons. Analysis showed that, on average, CA1 pyramidal neurons were inhibited slightly longer than CA3 pyramidal neurons, although the CA1 data set proved to be more variable. The median length of CA1 inhibition was 85.6 ms, which falls short of the 100 ms threshold used in the Jadhav et al. (2012) paper. It is important to mention the different methods used to calculate inhibition in each situation. We analyzed individual spiking activity from cells and cross-correlated their spiking to the onset of the stimulus to determine the total

length of time that the cells are transiently silenced for. After this is determined for one cell, this value would be averaged across all CA1 or CA3 cells recorded on tetrodes in those regions for each experiment. This is in contrast to the technique used by Jadhav et al. (2012). They analyzed the mean firing rate of CA1 pyramidal neurons, cross-referenced that with the stimulus artifact, and chose a threshold of inhibition based on the time it took the mean spiking rates to return back to a baseline firing rate similar to before the onset of the stimulus (Jadhav et al., 2012). This methodological difference may result in shorter duration obtained for our study because our duration of inhibition ends as soon as the cell begins to spike again whereas the other technique used by Jadhav et al. (2012) will likely result in a longer duration because it also includes the time after cells begin to fire again until they reach pre-stimulus baseline firing rates. Nonetheless, the ranges of inhibition obtained in our study are comparable to this previous study. We were also interested in seeing the relative duration of inhibition in CA3 pyramidal neurons at stimulation strengths that elicited ~100 ms inhibition in CA1. A linear regression analysis predicted 79 ms of CA3 inhibition for 100 ms of CA1 inhibition; although this value should be accepted cautiously as the inhibition data does not fit a linear distribution very well. In any case, CA3 inhibition seems to be consistently lower than CA1 inhibition at the same stimulation strengths. This discrepancy may be explainable by the differences in anatomy between the CA1 and CA3 regions; the CA3 region is generally more active and excitable than the CA1 region due to more synaptic connections from the CA3-CA3 recurrent pathway, larger pyramidal neurons (resulting in larger amplitude spikes observed on multiunit activity), and other hippocampal oscillations such as gamma waves. Nevertheless, figures 10 and 11 illustrated how duration of inhibition in the CA1 or CA3 pyramidal neurons was not correlated to memory performance on the 8-arm radial maze. Figure 12 shows the relative unimportance of the previously-used 100 ms

threshold for CA1 inhibition. Four out of 17 of our experiments had > 70% of all recorded CA1 pyramidal neurons inhibited > 100 ms, and no resulting impairment in memory performance was observed. A moderate decline in memory performance was observed with increased duration of CA3 inhibition, although this proved to be statistically insignificant. Since SWR events are known to reactivate large populations of pyramidal neurons in an excitatory burst, the goal of inducing cellular inhibition was to prevent the reactivation of place cells that may code for future trajectories to support the on-line decision making process. Although our results do not suggest a relationship exists between inhibition and memory performance, additional analysis should be done to determine how efficiently SWRs were disrupted after vHC stimulation. This factor must be considered as inhibition alone is not the most direct measure of SWR disruption success. Nonetheless, the inhibition duration that we induced is similar to previous experiments that have disrupted memory consolidation (Girardeau et al., 2009) and learning (Jadhav et al., 2012), but we do not observe impairments in spatial WM performance.

The next metric to analyze was SWR detection and stimulation efficiency. 74.1% (20/27) of our experiments had a SWR efficiency ≥ 85%, indicating a relatively high percentage of SWR events being detected and disrupted during awake behavior on the radial maze. The higher this percentage is for any SWR disruption experiment, the fewer SWRs escape our disruption algorithm. We arbitrarily decided to choose a threshold of 85% for our SWR efficiency value to include experiments in the analysis. Although some SWRs may escape our manipulation based on this threshold, if SWR events are truly necessary for spatial WM behavior, knocking out 85% or more of them during the task would logically result in a memory impairment relative to controls. Increased SWR efficiency did not result in increased deficits on the 8-arm radial maze task. This strongly indicates that SWR events are not necessary for spatial WM processes

because disruption of the vast majority of these events during the task does not impact memory performance on the radial maze. Conversely, lower SWR efficiency percentages (~65-75%) do not show improvements in performance on the maze, indicating that SWRs may not be necessary to facilitate spatial WM processes. One confounding variable here is the frequency of stimulations being delivered. Due to the inherent imperfections surrounding online detection and disruption of SWRs (view figure 4), all experiments will involve some degree of overstimulation. Therefore, any behavioral deficits during SWR disruption experiments should not immediately be attributed to selective disruption of SWRs without first accounting for the relative stimulation frequency compared to the 200 ms control experiment. This analysis has not yet been conducted, although a preliminary search of the data has indicated overstimulation is not solely to blame for decreased memory performance in some experiments, and it is also present in experiments where animals perform very well on the spatial WM task. Nonetheless, this seems to strengthen our hypothesis that SWRs are not necessary for spatial WM processes. Many experiments that have a very large mismatch between offline SWRs and online detection of them (inducing overstimulation) result in no obvious deficits in memory performance on the 8-arm radial maze.

No significant differences in memory performance were discovered “between” any of the disruption and 200 ms delay control experiments (comparisons analyzed by equal trial blocks, refer to figure 14). This is strong evidence to conclude that SWR disruption does not impair spatial WM abilities. However, the most important analysis to conduct is to assess the real-time effects that SWR disruption has on memory performance on the maze. We decided to test this by separating all trials within an experiment into trial blocks (NS1, S1, NS2, S2, NS3), alternating between no-stimulation (NS) trials and stimulation trials (S). This serves as the

ultimate test because disruption of SWRs can theoretically impair ongoing memory performance on a precise temporal basis if they do prove to be important for spatial WM processes. This experimental framework allows us to alternate between disruption and control trials to most effectively detect transient impairments when SWRs are disrupted. Upon initial comprehensive application of the Mann-Whitney U test, most temporal differences between groups proved to be non-significant (view table 1B, "within"). Of the 64 individual tests conducted, five proved to fall below the stated significance level of $\alpha = 0.05$ (view table 1B, these values are bolded and contain asterisks). To account for the multiple comparisons conducted and to reduce the chance of obtaining false positive results, a Holm-Bonferroni correction (H-Bc) was applied. After Holm-Bonferroni correction, these previously significant results all failed to reach the corrected significance levels (view table 1B, H-Bc column), indicating that they were obtained by chance. These findings strongly suggest that SWRs generated in the CA1 or CA3 region do not subserve spatial WM processes because disruption of these events do not impair memory performance on the 8-arm radial maze. Although we can confidently conclude that CA3 SWRs are not involved in spatial WM processes, our CA1 data set contains smaller sample sizes collected from a limited number of animals, preventing us from concluding that CA1 SWRs are not important for spatial WM.

One important finding relates to the NS3 performance for all experimental groups. As can be seen on both graphs in figure 14A and 14B, rats often finish experiments with very high NS3 % correct averages. The reasons for this are unclear; perhaps rats become insensitive to the stimulus, or perhaps their performance simply just trends upwards throughout the experiment. Either way, this pattern should be explored in further detail in future analysis.

All of our results indicate no significant impairment in spatial WM performance without SWR events. Therefore it is important to consider the relative lack of impairment in memory performance on the maze when SWR events are disrupted compared to other deficit experiments. DG-lesioned animals in the Sasaki et al. (2018) study performed drastically worse (ranging from 18.4 % to 45.3% over 6 days) than their control counterparts (39.6 % to 78.2%). Another potentially more applicable comparison can be conducted against the earliest WM training sessions that all of the nine rats included in the analysis took part in. This "novice" memory performance was calculated based on the combined average percent correct (M = 62.0, SD = 9.4) from 27 total days collected from nine animals during the first three days of radial maze training after habituation. None of the averages from any of the SWR disruption or control groups came anywhere near this level of impairment.

In conclusion, our causal disruption of SWR events in the CA3 region failed to demonstrate memory impairment on a spatial WM task. This result was unexpected considering previous findings by Pfeiffer & Foster (2013) motivated a whole field of research that assumed SWRs were necessary to guide ongoing behavior towards the next goal location in complex spatial tasks. Therefore, contrary to this popular belief in the field, our results indicate SWR events are not the primary mechanism for guiding hippocampal-dependent spatial WM behavior. It seems implausible that SWR events are solely responsible for facilitating spatial WM abilities during awake behavior due to the infrequency of these events during locomotion outside of the reward zone. A recent study published in 2021 by Gillespie et al. (2021) provides corroborating evidence that awake-SWR events facilitate memory consolidation processes rather than planning behavior towards future goal locations, even when SWR events include place cell representations for future locations. They postulated that neuronal ensembles are strengthened during SWR

events, and that these ensembles can be later expressed and used in a flexible manner during other hippocampal states to guide spatial behavior (Gillespie et al., 2021). Perhaps the true function of the hippocampal SWR is to take a "snapshot" of the current spatial environment to code this information into long-term memory through a synaptic plasticity-mediated process. It would make sense that this "uploading" process of spatial information into the cognitive network would only occur sporadically during awake behavior, especially when rewards are not currently being discovered or consumed. Rewards serve as strong motivators, which potentially explains why Ambrose et al. (2016) found that reverse replay events during SWRs can be modulated by the relative size of the reward received. As for forward replay events observed during SWRs before behavior, it may be the case that the SWR functions in a similar manner to upload the current information into the cognitive network in order to consolidate that memory for later use. Fundamentally, the SWR is a population level excitation burst of pyramidal neurons in the hippocampal cell layers in a time-compressed sequence. Theta phase precession is another popular mechanism that may underlie spatial WM processes. This involves the ordered firing of place cells during theta states as animals traverse an environment (O'Keefe & Recce, 1993). Considering that theta waves are continuously observed during waking behavior and REM sleep, and that they increase in frequency during locomotion in spatial WM tasks such as the 4-arm radial maze (Belchior et al., 2014), it seems that theta states are much more related to ongoing decision making than are SWRs. Early work by Mitchell et al. (1982) demonstrates a necessary role for theta oscillations in a working-memory version of the eight-arm radial maze task. This further supports the notion that theta oscillations are likely more involved in working memory tasks as compared to SWR events. Considering that SWRs are important for learning and consolidation of memories (Jadhav et al., 2012; Girardeau et al., 2009), it seems plausible that

SWR events are necessary to encode the surrounding spatial environment into long term memory so spike activity patterns during theta states can guide ongoing decision making processes in spatial environments. For these reasons, future research should analyze theta states and SWRs in tandem to truly understand how these two mechanisms cooperate to support ongoing decision making during complex spatial WM tasks.

CHAPTER IV – CONCLUSION

In summary, we have demonstrated that disruption of pyramidal cell activity during CA3 SWR events does not induce deficits in spatial WM abilities on a dentate-dependent 8-arm radial maze. This finding is surprising considering previous research showing a role for SWRs in the reactivation of place cells that code for future goal locations within an environment. We conclude that SWR events do not mechanistically support spatial WM processes while a rat conducts a hippocampal-dependent task. Future research should consider other hippocampal oscillatory events like theta states or gamma oscillations that may play a more important and frequent role in coordinating neuronal activity to guide animals to future reward locations in a spatial environment.

This thesis is currently being prepared for submission of publication of the material by Zhang, Yuhan; Taylor, Brandon; Leutgeb, Stefan; Leutgeb, Jill. The author of this thesis will be a co-author of the publication.

REFERENCES

Amaral, D. G., Scharfman, H. E., & Lavenex, P. (2007). The dentate gyrus: fundamental neuroanatomical organization (dentate gyrus for dummies). Progress in brain research, 163, 3–22. https://doi.org/10.1016/S0079-6123(07)63001-5.

Ambrose, R. E., Pfeiffer, B. E. & Foster, D. J. (2016). Reverse replay of hippocampal place cells is uniquely modulated by changing reward. Neuron, 91(5), 1124–1136. doi: 10.1016/j.neuron.2016.07.047

Belchior, H., Lopes-Dos-Santos, V., Tort, A. B., & Ribeiro, S. (2014). Increase in hippocampal theta oscillations during spatial decision making. Hippocampus, 24(6), 693–702. https://doi.org/10.1002/hipo.22260

Bliss, T.V., & Collingridge, G.L. (1993). A synaptic model of memory: long-term potentiation in the hippocampus. Nature, 361:31–39. doi: 10.1038/361031a0.

Butler, J. L., & Paulsen, O. (2015). Hippocampal network oscillations — recent insights from in vitro experiments. Current Opinion in Neurobiology, 31, 40-44. https://doi.org/10.1016/j.conb.2014.07.025

Buzsáki, G. (2015). Hippocampal sharp wave-ripple. A cognitive biomarker for episodic memory and planning. Hippocampus, 25(10), 1073–1188. https://doi.org/10.1002/hipo.22488

Colgin, L. L., & Moser, E. I. (2010). Gamma Oscillations in the Hippocampus. Physiology, 25: 319- 329. https://doi.org/10.1152/physiol.00021.2010

Csicsvari, J., Hirase, H., Czurkó, A., Mamiya, A., & Buzsáki, G. (1999). Fast network oscillations in the hippocampal CA1 region of the behaving rat. The Journal of neuroscience: the official journal of the Society for Neuroscience, 19(16), RC20. https://doi.org/10.1523/JNEUROSCI.19-16-j0001.1999

Dannenberg, H., Kelley, C., Hoyland, A., Monaghan, C. K., & Hasselmo, M. E. (2019). Journal of Neuroscience, 39(18), 3434-3453. https://doi.org/10.1523/JNEUROSCI.1450-18.2019

Dudek, S. M., Alexander, G. M., & Farris, S. (2016). Rediscovering area CA2: unique properties and functions. Nature reviews. Neuroscience, 17(2), 89–102. https://doi.org/10.1038/nrn.2015.22

Foster, D., Wilson, M. (2006). Reverse replay of behavioural sequences in hippocampal place cells during the awake state. Nature 440, 680–683. https://doi.org/10.1038/nature04587

Gillespie, A. K., Maya, D. A. A., Denovellis, E. L., Roumis, D. K., Eden, U. T., & Frank, L. M. (2021). Hippocampal replay reflects specific past experiences rather than a plan for

subsequent choice. Neuron, 109(19), 3149-3163. DOI:https://doi.org/10.1016/j.neuron.2021.07.029

Girardeau, G., Benchenane, K., Wiener, S. I., Buzsáki, G., & Zugaro, M. B. (2009). Selective suppression of hippocampal ripples impairs spatial memory. Nature Neuroscience, 12, 1222-1223. https://doi.org/10.1038/nn.2384

Green, J. D. (1964). The Hippocampus. In Physiological reviews Vol. 44, pp. 561–608. https://doi.org/10.1152/physrev.1964.44.4.561

Hafting, T., Fyhn, M., Molden, S., Moser, M. B., & Moser, E. I. (2005). Microstructure of a spatial map in the entorhinal cortex. Nature, 436, 801–806. https://doi.org/10.1038/nature03721

Hitti, F., & Siegelbaum, S. (2014). The hippocampal CA2 region is essential for social memory. Nature 508, 88–92. https://doi.org/10.1038/nature13028

Insausti, R., Annese, J., Amaral, D. G., & Squire, L. R. (2013). Human amnesia and the medial temporal lobe illuminated by neuropsychological and neurohistological findings for patient E.P. Proceedings of the National Academy of Sciences of the United States of America, 110(21), 1953–1962. https://doi.org/10.1073/pnas.1306244110.

Jadhav, S. P., Kemere, C., German, P. W., & Frank, L. M. (2012). Awake hippocampal sharp wave ripples support spatial memory. Science, 336(6087), 1454–1458. https://doi.org/10.1126/science.1217230

Joo, H. R., & Frank, L. M. (2018). The hippocampal sharp wave-ripple in memory retrieval for immediate use and consolidation. Nature Reviews Neuroscience, 19(12):744-757. doi: 10.1038/s41583-018-0077-1

Killian, N., Jutras, M. J., & Buffalo, E. A. (2012). A map of visual space in the primate entorhinal cortex. Nature, 491, 761-764. doi: 10.1038/nature11587.

Knierim, J. J., Neunuebel, J. P., & Deshmukh, S. S. (2013). Functional correlates of the lateral and medial entorhinal cortex: objects, path integration and local–global reference frames. Philos Trans R Soc Lond B Biol Sci. 369(1635): 20130369. doi: 10.1098/rstb.2013.0369.

Lashley, K. S. (1950). In search of the engram. In Society for Experimental Biology, Physiological mechanisms in animal behavior. (Society's Symposium IV.) (pp. 454–482). Academic Press.

Leutgeb, S., Leutgeb, J. K., Barnes, C. A., Moser, E. I., McNaughton, B. L., & Moser, M. B. (2005). Independent codes for spatial and episodic memory in hippocampal neuronal ensembles. Science (New York, N.Y.), 309(5734), 619–623. https://doi.org/10.1126/science.1114037

Leutgeb, J. K., Leutgeb, S., Moser, M. B., & Moser, E. I. (2007). Pattern separation in the dentate gyrus and CA3 of the hippocampus. Science, 315(5814), 961-966. https://doi.org/10.1126/science.1135801

MacDonald, C. J., Lepage, K. Q., Eden, U. T., & Eichenbaum, H. (2011). Hippocampal "time cells" bridge the gap in memory for discontiguous events. Neuron, 71(4), 571-573. https://doi.org/10.1016/j.neuron.2011.07.012

Mitchell, S. J., Rawlins, J. N., Steward, O, & Olton, D. S. (1982). Medial septal area lesions disrupt theta rhythm and cholinergic staining in medial entorhinal cortex and produce impaired radial arm maze behavior in rats. Journal of Neuroscience, 2(3), 292-302. DOI: https://doi.org/10.1523/JNEUROSCI.02-03-00292.1982

Morris, R. G., Garrud, P., Rawlins, J. N., & O'Keefe, J. (1982). Place navigation impaired in rats with hippocampal lesions. Nature, 297(5868), 681–683. https://doi.org/10.1038/297681a0

Nádasdy, Z., Hirase, H., Czurkó, A., Csicsvari, J., Buzsáki, G. (1999). Replay and Time Compression of Recurring Spike Sequences in the Hippocampus. Journal of Neuroscience, 19(21), 9497-9507; doi: 10.1523/JNEUROSCI.19-21-09497.1999

Nakashiba, T., Buhl, D. L., McHugh, T. J., & Tonegawa, S. (2009). Hippocampal CA3 output is crucial for ripple-associated reactivation and consolidation of memory. Neuron, 62(6), 781–787. https://doi.org/10.1016/j.neuron.2009.05.013.

Newrzella, D., Pahlavan, P. S., Krüger, C., Boehm, C., Sorgenfrei, O., Schröck, H., Eisenhardt, G., Bischoff, N., Vogt, G., Wafzig, O., Rossner, M., Maurer, M. H., Hiemisch, H., Bach, A., Kuschinsky, W., & Schneider, A. (2007). The functional genome of CA1 and CA3 neurons under native conditions and in response to ischemia. BMC genomics, 8, 370. https://doi.org/10.1186/1471-2164-8-370

Novitskaya, Y., Sara, S. J., Logothetis, N. K., & Eschenko, O. (2016). Ripple-triggered stimulation of the locus coeruleus during post-learning sleep disrupts ripple/spindle coupling and impairs memory consolidation. Learning & memory, 23(5), 238–248. https://doi.org/10.1101/lm.040923.115

Nuñez, A., & Buño, W. (2021). The Theta Rhythm of the Hippocampus: From Neuronal and Circuit Mechanisms to Behavior. Frontiers in Cellular Neuroscience, 15. https://doi.org/10.3389/fncel.2021.649262

O'Keefe, J. (1976). Place units in the hippocampus of the freely moving rat. Experimental Neurology, 51(1), 78-109. https://doi.org/10.1016/0014-4886(76)90055-8

O'Keefe, J., & Recce, M. L. (1993). Phase relationship between hippocampal place units and the EEG theta rhythm. Hippocampus, 3(3), 317–330. https://doi.org/10.1002/hipo.450030307

Oliva, A., Fernández-Ruiz, A., Buzsáki, G., & Berényi, A. (2016). Role of Hippocampal CA2

Region in Triggering Sharp-Wave Ripples. Neuron, 91(6), 1342–1355. https://doi.org/10.1016/j.neuron.2016.08.008

Penfield W., & Boldrey E. (1937). Somatic motor and sensory representation in the cerebral cortex of man as studied by electrical stimulation. Brain, 60(4), 389-443. https://doi.org/10.1093/brain/60.4.389

Pfeiffer, B. E., & Foster, D. J. (2013). Hippocampal place-cell sequences depict future paths to remembered goals. Nature, 497(7447), 74–79. https://doi.org/10.1038/nature12112

Sadowski, J. H., Jones, M. W., & Mellor, J. R. (2016). Sharp-Wave Ripples Orchestrate the Induction of Synaptic Plasticity during Reactivation of Place Cell Firing Patterns in the Hippocampus. Cell reports, 14(8), 1916–1929. https://doi.org/10.1016/j.celrep.2016.01.061

Sasaki, T., Piatti, V. C., Hwaun, E., Ahmadi, S., Lisman, J. E., Leutgeb, S., & Leutgeb, J. K. (2018). Dentate network activity is necessary for spatial working memory by supporting CA3 sharp-wave ripple generation and prospective firing of CA3 neurons. Nature neuroscience, 21(2), 258–269. https://doi.org/10.1038/s41593-017-0061-5

Schultz, C., & Engelhardt, M. (2014). Anatomy of the hippocampal formation. Karger Publishers. https://www.karger.com/Article/Pdf/360925

Scoville, W. B., & Milner, B. (1957). Loss of recent memory after bilateral hippocampal lesions. Journal of neurology, neurosurgery, and psychiatry, 20(1), 11–21. https://doi.org/10.1136/jnnp.20.1.11

Solstad, T., Boccara, C., Kropff, E., Moser, M. B., & Moser, E. I. (2008). Representation of geometric borders in the entorhinal cortex. Science, 322(5909), 1865-1868. https://doi.org/10.1126/science.1166466

Squire L. R. (2009). The legacy of patient H.M. for neuroscience. Neuron, 61(1), 6–9. https://doi.org/10.1016/j.neuron.2008.12.023

Van Groen, T., & Wyss, J. M. (1990). Extrinsic projections from area CA1 of the rat hippocampus: olfactory, cortical, subcortical, and bilateral hippocampal formation projections. The Journal of comparative neurology, 302(3), 515–528. https://doi.org/10.1002/cne.903020308

Whitlock, J. R., Heynen, A. J., Shuler, M. G., & Bear, M. F. (2006). Learning induces long-term potentiation in the hippocampus. Science, 313(5790), 1093-1097. doi:10.1126/science.1128134.

Wierzynski, C. M., Lubenov, E. V., Gu, M., & Siapas, A. G. (2009). State-Dependent Spike-Timing Relationships between hippocampal and prefrontal circuits during sleep. Neuron, 61(4), 587-596. https://doi.org/10.1016/j.neuron.2009.01.011

Witter, M. P., Doan, T. P., Jacobsen, B., Nilssen, E. S., & Ohara, S. (2017). Architecture of the Entorhinal Cortex A Review of Entorhinal Anatomy in Rodents with Some Comparative Notes. Frontiers in systems neuroscience, 11, 46. https://doi.org/10.3389/fnsys.2017.00046

Xavier, G. F. & Costa, I. V. (2009). Dentate gyrus and spatial behaviour. Progress in neuro-psychopharmacology & biological psychiatry, 117(33), 762-773. https://doi.org/10.1016/j.pnpbp.2009.03.036

Yamada, J. & Jinno, S. (2021). Potential involvement of perineuronal nets in brain aging: an anatomical point of view. Factors Affecting Neurological Aging, 163-172. https://doi.org/10.1016/B978-0-12-817990-1.00015-9.